HIGH-VALENT METAL-OXO SPECIES: Iron and Manganese Oxo Complexes, Oxo Wall and Beyond

Virginia Larson
Department of Chemistry and Department of Biophysics, University of Michigan, 930 North University Avenue, Ann Arbor, MI 48109-1055.

Beatrice Battistella
Department of Chemistry, Humboldt-Universität zu Berlin, Brook-Taylor-Strasse 2, Berlin, Germany

Kallol Ray*
Department of Chemistry, Humboldt-Universität zu Berlin, Brook-Taylor-Strasse 2, Berlin, Germany 12489. Email: kallol.ray@chemie.hu-berlin.de

Nicolai Lehnert*
Department of Chemistry and Department of Biophysics, University of Michigan, 930 North University Avenue, Ann Arbor, MI 48109-1055. Email: lehnertn@umich.edu

Wonwoo Nam*
Department of Chemistry and Nano Science, Ewha Womans University, Seoul 03760, Korea.
School of Chemistry and Chemical Engineering, Shaanxi Normal University, Xi'an 710119, China. Email: wwnam@ewha.ac.kr

I. Abstract

High-valent metal-oxo species with multiple metal-oxygen bonds are one of the key intermediates proposed in many catalytic cycles of biological and abiological oxidation reactions. These intermediates have been implicated as active oxidants in alkane hydroxylation, olefin epoxidation, and other oxidation reactions. For example, iron(IV)-oxo porphyrin π-cation radicals are used to oxidize organic substrates in Cytochrome P450s, a class of enzymes common to many life forms. High-valent manganese-oxo species are reported to be active in the oxidation of water in Photosystem II. Both of these examples in Nature have spurred chemists to model highly oxidized transition metal complexes. Indeed, many examples of iron- and manganese-oxo complexes have now been reported, but analogs of the late transition metals, groups 9 – 11, are rare. In addition, late transition metal-oxo complexes in a tetragonal (four-fold) symmetry should be electronically unstable, a rule commonly referred to as the "oxo wall". However, by using other symmetries or spin states, a few of these reactive compounds of the late transition metals have been synthesized and studied using spectroscopic methods in correlation with theoretical investigations. This review highlights the mononuclear non-heme iron- and manganese-oxo species, the nature of the "oxo wall", and the recent advances in the late transition metal-oxo complexes of cobalt, nickel, and copper.

II. Introduction

Transition metal-mediated O−O bond formation and cleavage reactions are involved in a variety of biological and chemical oxidation reactions, which are relevant for many processes related to renewable energy.[1–14] High-valent metal-oxo complexes often act as common reactive intermediates in many of these oxidation reactions. Nature mainly uses iron and manganese for these transformations, due to their availability, appropriate binding of oxygen species, and rich redox chemistry.[12,15] These findings inspired in-depth studies of Mn- and Fe-oxo systems and

from there, these studies have been extended to similar systems with later transition metals. For example, the O-O bond formation step leading to the evolution of dioxygen in the oxygen evolving complex (OEC) in Photosystem II (PS II) is proposed to occur via a transient but not isolated manganese-oxo intermediate (Figure 1a).[16–20] The Mn oxidation states and the mechanism of O-O bond formation remain, however, elusive. Two mechanisms for the formation of O-O bond at metal-oxo active sites have been proposed; the acid–base mechanism involves the attack of a nucleophilic oxygen species (i.e., H_2O) on an electrophilic metal-oxo species (Figure 1b). For the radical coupling mechanism (Figure 1b), two high-valent metal-oxos containing sufficient spin densities on the oxygen atoms are needed to drive O-O bond coupling. Detailed experimental and theoretical mechanistic studies to discern between the two possible O-O bond formation mechanisms have previously yielded controversial results,[21,22] though recent work favors an oxyl/oxo coupling mechanism.[23,24] The major problem is the absence of any isolable intermediates associated with the O-O bond formation step, which prevents the unambiguous assignment of the mechanism(s). This continues to inspire bioinorganic chemists to synthesize and study model complexes.

The mechanism of the microscopic reverse process, which is the activation of dioxygen to generate high-valent metal-oxo intermediates via homolytic or heterolytic O-O bond cleavage of initially formed metal-dioxygen intermediates, is better understood.[11–14] This understanding has been aided by the trapping and in-depth spectroscopic characterization of the various high-valent iron-oxo cores in heme and non-heme oxygenases, which can undergo hydroxylations, O-atom transfers, and other reactions (Figure 1C).[12,25–27] In alkane hydroxylation reactions, the iron-oxo intermediate abstracts a hydrogen atom (H-atom) from substrates to generate a substrate radical and iron-hydroxide, which can either undergo a fast recombination to yield a hydroxylated product via an oxygen-rebound mechanism or performs a second H-atom abstraction leading to desaturation product.[28] A mononuclear iron(IV)-oxo intermediate *J* has been identified in the catalytic cycle of taurine dioxygenase as a kinetically competent oxidant for the hydroxylation of taurine (Figure 1a).[29] Similarly, a dinuclear iron(IV)-oxo species is believed to be the active oxidant responsible for the hydroxylation of methane in soluble methane oxygenase (*s*MMO).[30,31] However, the structure of the active oxidant in *s*MMO has been controversially discussed in the literature. While initial resonance Raman (rRaman) investigations[30] suggested a diamond core $Fe^{IV}_2O_2$ structure, recent Kα high-energy resolution fluorescence detected (HERFD) X-ray absorption spectroscopy[31] revealed a large Fe-Fe distance of 3.9 Å, consistent with an open core $O{=}Fe^{IV}{-}O{-}Fe^{IV}{=}O$ assignment (Figure 1a). The involvement of high-valent iron-oxo cores in iron-mediated biological oxidation reactions also inspired chemists to implicate high-valent copper-oxo cores in the mechanisms of copper-mediated biological oxidation reactions (Figure 1a).[32–35] For example, terminal copper(III)-oxo and bis(μ-oxo)dicopper(III) cores have been suggested as reactive intermediates responsible for the oxidative C-H bond cleavage of biopolymers and other substrates, including methane, at the active sites of mononuclear and coupled and non-coupled dinuclear copper-oxygenases. However, direct evidence of such intermediates is rare, and a Cu^{III} oxidation state has not yet been definitively assigned to any redox mechanisms in biology.

The uncertainty related to the O-O bond formation mechanism in PS II and the nature of the reactive intermediates in many iron- and copper-containing oxygenases inspired bioinorganic chemists to simulate corresponding structural motifs (Figure 1c). In using molecular complexes for the O-O bond formation and cleavage reactions they obtain a better understanding of the biological oxidation reactions. Studies have also extended beyond Nature's choice of transition metals for these reactions, such as manganese, iron, and copper. In total, this has led to the synthesis of a large variety of bioinspired and biomimetic chromium, manganese, iron, cobalt, nickel, and copper complexes,[9,12–14,25,36–39] some of which have provided valuable spectroscopic models for the enzymatic active sites. In addition, a few heavy late transition metal complexes have been prepared and studied.[40,41] The reactivity of high-valent Mn-, Fe-, Co-, Ni-, and Cu-

oxo cores towards O-O bond formation, hydrogen atom transfer (HAT), and oxygen atom transfer (OAT) reactions has also been investigated. In the nickel and copper chapters, evidence for such high-valent intermediates is discussed. In this review, we will discuss milestones that have been achieved in the last 5 – 10 years for the mononuclear non-heme chemistry involving the first row, high-valent transition metal-oxo complexes beginning with the better studied Mn and Fe species used in Nature and continuing to the late transition metals Co, Ni, and Cu.

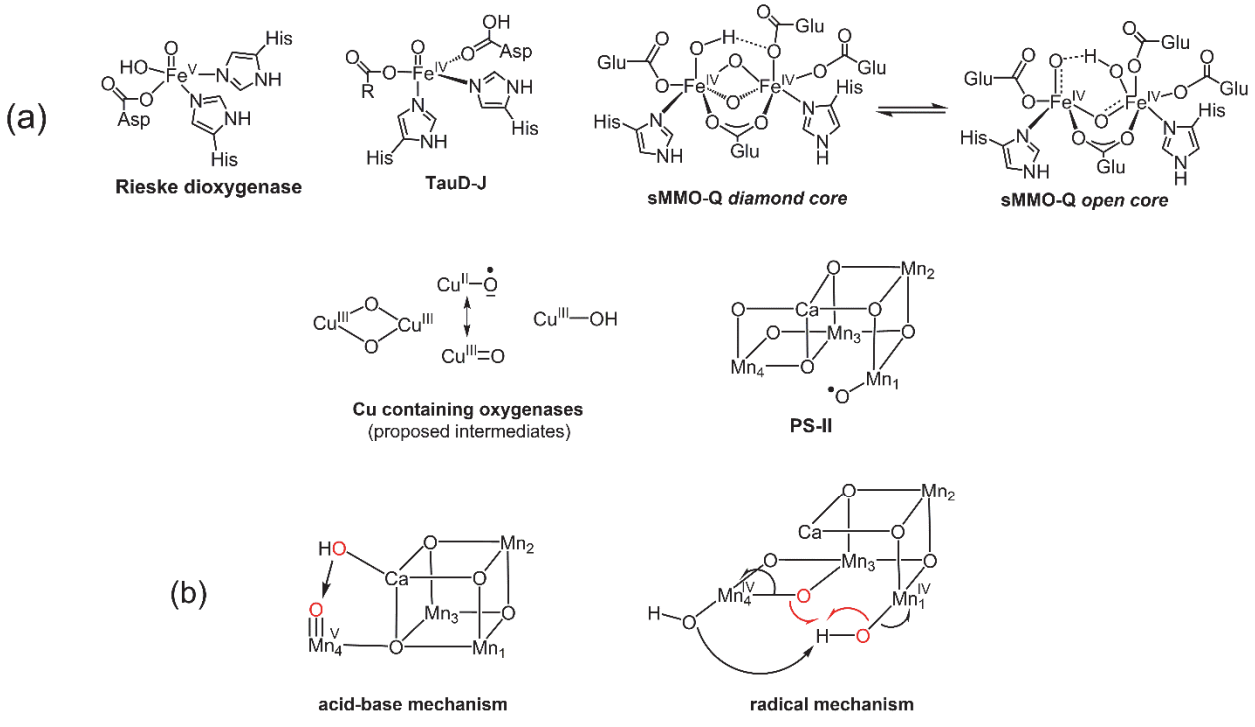

Figure 1. Selected high-valent biological intermediates (a), proposed mechanisms of dioxygen evolution at the oxygen-evolving complex (OEC) in Photosystem II (PS II) (b), and reactivities of biologically relevant iron-oxo species (c).

III. Metal–Oxo Bonding and the Oxo Wall

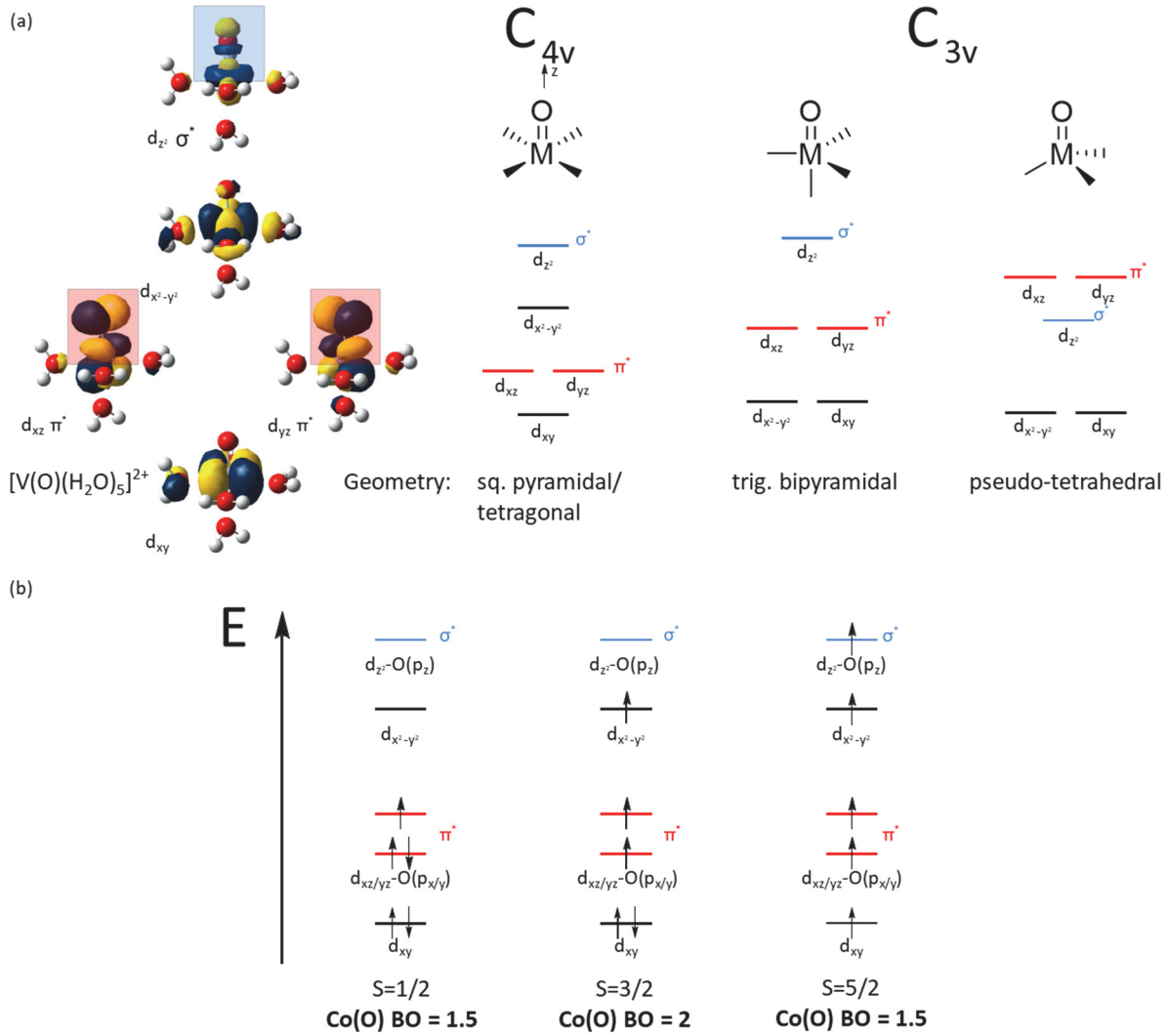

Figure 2. (a) The d-orbital splittings in the effective symmetries often found in metal-oxo complexes. Molecular orbitals calculated for $[V(O)(H_2O)_5]^{2+}$ are included under tetragonal (C_{4v}) symmetry, to indicate σ- and π-bonding interactions between the metal and the oxo ligand. The Co-oxo σ- and π–antibonding interactions are highlighted. Here, the M-O bond constitutes the *z* axis of the complex. (b) Effect of different spin states on the formal bond order (BO) in tetragonal Co(IV)-oxo complexes.

The reactivity and stability of terminal metal-oxo cores can be derived from simple ligand-field theory considerations. To understand the bonding between the metal center and the oxo ligand, one first needs to evaluate the relevant metal and ligand orbitals involved in the bond. For the oxo dianion (O^{2-}), the occupied valence 2p orbitals can make σ- and π-donor bonds to the metal center. For the first row transition metals, 3d-orbitals are the most relevant for bonding, especially for highly oxidized metal centers. The d-orbitals split in energy by the ligand field

created by all of the ligands coordinated to the metal center. In an octahedral ligand field, the d_{z2} and d_{x2-y2} orbitals that overlap directly with the ligands are raised in energy relative to the d_{xy}, d_{xz}, and d_{yz} orbitals. If one of the metal-ligand bonds is significantly stronger than the other ones, such as in the case of a metal-oxo compound, effective tetragonal or C_{4v} symmetry results. In C_{4v} symmetry, the metal-oxo bond is aligned with the *z*-axis. Compared to the d_{xy} orbital, the d_{xz} and d_{yz} orbitals are distinctively raised in energy due to their π-antibonding interactions with the oxo group. Likewise, the d_{z2} is raised due to the strong M-O σ-bonding interaction. This leads to the MO diagram shown in Figure 2a, left. In most cases, the d_{xy} orbital is essentially non-bonding with respect to all ligands. The d_{x2-y2} orbital is in the *xy* plane, perpendicular to the metal-oxo bond, and makes σ bonds with the other ligands, whose electron donating or withdrawing abilities provide a good way to tune the properties of the metal-oxo complexes.

The average energy of the d-orbitals, which depends on the effective nuclear charge of the metal cation, decreases (a) across the first row (from left to right) and (b) with increasing oxidation state of the metal. This means that for early transition metals, the filled 2p orbitals of the oxo group are much lower in energy than the metal 3d-orbitals. Therefore, when the bonding and antibonding M-O orbitals form, the bonding combinations are mostly localized on the oxo anion and the antibonding combinations are identified with the metal d-orbitals (see Figure 2a, left). Going across the periodic table towards the late transition metals, the covalency of the metal-oxo bond then increases, as the d-orbitals shift to lower energy.

In the MO diagram for C_{4v} symmetry, leftmost in Figure 2a, the electrons of the oxo group formally occupy the bonding metal-oxo orbitals (at lower energy and not shown). The number of electrons in the d-orbitals then depends on the nature and oxidation state of the metal. In $[V(O)(H_2O)_5]^{2+}$, initially studied by Ballhausen and Gray in 1962,[42] vanadium is in the +4 state, and in the resulting d^1 system, the single d-electron is placed in the non-bonding d_{xy} orbital. This gives a formal vanadium-oxo triple bond. Advancing across the first row increases the electron count. In a tetragonal Cr(IV)-oxo (d^2) complex, a second electron is added to d_{xy}. For Mn(IV)-oxo (d^3), a first electron is now added to the M-O antibonding π^* orbitals (d_{xz}/d_{yz}), decreasing the formal M-O bond order to 2.5 (and causing a Jahn-Teller distortion). For Fe(IV)-oxo (d^4), which is a key intermediate in C-H bond activation by high-valent heme and non-heme iron-oxo intermediates (see Introduction), the famous Fe(IV)=O double bond results. Then, one hits the oxo wall. Advancing from iron(IV) to cobalt(IV) adds another electron to an M-O π antibonding orbital, decreasing the bond order to 1.5. As the bond order decreases, the oxo ligand becomes more and more basic and nucleophilic. This destabilizes the metal-oxo unit making it much more reactive, leading to protonation and/or formation of bridged M-O-M units. With substrates available, this likely increases reactivity for OAT and HAT, as mentioned in the Introduction and discussed further below. The problem of decreasing bond order only worsens as one adds additional antibonding electrons for nickel and copper. This instability and corresponding increased reactivity was first noted by Ballhausen and Gray, along with their detailed analysis of the vanadyl-oxo bond in 1962, which is now widely known as the “oxo wall”.[3,43] This term was coined by Harry Gray in the 1990s and first used in his advanced inorganic chemistry course.[44]

The discussion so far has focused on low-spin (ls) complexes. There is, however, a possibility to **break the oxo wall** if higher spin states are considered, at least in the case of Co(IV). Figure 2b shows simplified MO diagrams of tetragonal, formally Co(IV)-oxo complexes, in different spin states to illustrate this concept. The diagrams illustrate that a Co(IV) center in an intermediate spin state (S = 3/2) is actually able to form a Co-oxo double bond – a direct violation of the oxo wall. One example for such a complex is $[Co(13\text{-TMC})(O)]^{2+}$ (13-TMC = 1,4,7,10-tetramethyl-1,4,7,10-tetraazacyclotridecane), as described below.[45] In the case of a Ni(IV)-oxo complex in the high-spin (hs) state (S = 2), a maximum Ni-O bond order of 1.5 could still be achieved. However, whether this latter type of complexes can be accessed experimentally is unclear.

A strategy to **circumvent the oxo wall** is to change the symmetry of the complex. Since the oxo wall is based on tetragonal symmetry, this strategy does not breach the oxo wall, despite corresponding claims in the literature. For example, in trigonal-bipyramidal (TBP) C_{3v} symmetry, a different splitting pattern of the d-orbitals results as shown in Figure 2a, middle. Here, the lowest-energy d-orbitals are d_{x2-y2} and d_{xy}, both perpendicular to the metal-oxo bond. Hence, four electrons can be stored in these d-orbitals (in the ls state), without affecting the (formal) metal-oxo bond order. In the case of Co(IV) and Ni(IV) complexes, one and two additional electrons are added to the π-antibonding d_{xz} and d_{yz} orbitals, which leads to the formal metal-oxo bond orders of 2.5 and 2, respectively. With Cu(IV), a third electron is added to these orbitals, destabilizing the metal-oxo bond to a maximum formal bond order of 1.5. Researchers have attempted to prepare a Co(IV)-oxo complex with TBP symmetry, but so far, only one example with a Lewis acid bound to the oxo group could be obtained (see below).[46]

Starting from TBP symmetry and removing the trans ligand to the oxo group allows the three remaining ligands to bend down, giving rise to pseudo-tetrahedral (PTD) C_{3v} symmetry (see Figure 2a, right). PTD leads to a similar orbital ordering as TBP, but the d_{z2} orbital could potentially drop in between the d_{x2-y2}/d_{xy} and d_{xz}/d_{yz} pairs, by mixing with the metal 4s and 4p orbitals as proposed for an iron-nitrido complex.[47] On the other hand, density functional theory (DFT) calculations on PTD vanadium- and chromium-oxo complexes predict d_{z2} to be the highest energy d-orbital in TBP symmetry,[48] so this point requires further study. In the former case, Co(IV)- and Ni(IV)-oxo complexes in the ls state would then lead to the population of the σ-antibonding d_{z2} orbital *before* population of the π-antibonding d_{xz}/d_{yz} orbitals, which would be a truly unique bonding situation. Notably, in 1993, a heavy late transition metal complex with this symmetry, $[Ir^{V}(O)(mesityl)_3]$, was synthesized and characterized.[40]

Another potential contributor to the lack of stability of the late transition metal-oxo complexes is valence tautomerization, leading to the formation of metal-oxyl ($O^{\bullet -}$) complexes, which are expected to be much more reactive (and less stable) than their metal-oxo valence tautomers.[49,50] This is particularly likely for late transition metal-oxo complexes, where the d-orbitals are already very low in energy. If the d-orbitals drop in energy below the occupied oxo(2p) donor orbitals, a so-called “bonding inversion” results, which means that now the metal-oxo bonding orbital combinations have more dominant metal contributions, and the antibonding orbital combinations have more ligand character.[50,51] In this way, the oxo ligand obtains distinct radical (oxyl) character, and a weaker metal-O bond results, which both lead to an activation of the metal-O group for further reactivity.

Examples of mononuclear non-heme metal-oxo complexes of the first transition metal ions from Mn to Cu are provided below, and their electronic structures and reactivities are discussed as well.

IV. Mononuclear Non-Heme Metal-Oxos of Fe and Mn

Iron- and manganese-oxo complexes bearing non-heme ligands have been well investigated over the past two decades. In this section, the characterization, electronic structure, reactivity, and implications for biological systems of these complexes are discussed. Analysing these isolable complexes helps researchers better understand unstable metal-oxo complexes in late transition metals.

a. Terminal Iron-Oxo Complexes

The first generation of a metastable non-heme iron(IV)-oxo complex, $[(cy\text{-}ac)Fe^{IV}(O)(CF_3SO_3)]^+$ (cy-ac = 1,4,8,11-tetraazacyclotetradecane-1-acetate), which employs an N4-cyclam (cyclam = 1,4,8,11-tetraazacyclotetradecane) ligand is shown in Figure 3a.[52] An S = 1 Fe(IV) assignment with an electronic configuration of $(d_{xy})^2(d_{xz})^1(d_{yz})^1$ was proposed based on Mössbauer data with an isomer shift (δ) of 0.1 mm s^{-1} and a quadrupole splitting (ΔE_Q) of 1.39 mm s^{-1} (Table 1 and SI, Table S1). Later, a modified cyclam ligand was employed to report the first X-ray crystal structure of a mononuclear non-heme S = 1 iron(IV)-oxo complex, $[(TMC)Fe^{IV}(O)(CH_3CN)]^{2+}$

(TMC = 1,4,8,11-tetramethyl-1,4,8,11-tetraazacyclotetradecane) (Figure 3a).[53] Since then, a large number of mononuclear non-heme iron(IV)-oxo complexes have been reported by utilizing a wide range of strong field nitrogen-rich or carbene-based polydentate ligands,[12,14,25] which stabilize the *S* = 1 ground state of the d^4 Fe(IV) center. In contrast, enzymatic non-heme iron(IV)-oxo cores possess an *S* = 2 ground state,[13,14,54] presumably because of the binding of the weak field carboxylate donors at their iron active sites. By enforcing a C_3 symmetry about the iron(IV) center, however, it has been possible to stabilize a few synthetic *S* = 2 iron(IV)-oxo units with a $(d_{x2-y2},d_{xy})^2(d_{xz})^1(d_{yz})^1$ electronic configuration[12,55–59] (Figure 3a). In both *S* = 1 and *S* = 2, the iron-oxo bond is a formal double bond as the π-antibonding orbitals are both singly occupied. For these high-valent Fe-oxo complexes, detailed analyses of their electronic structures as a function of spin- and oxidation state are available in the literature.[12–14,55,57,58] Although common synthetic procedures involve the reaction of the reduced iron complexes, $[LFe^{2+}]$, with oxo transfer agents, [O], such as iodosylbenzene (PhIO), N_2O, and peracids, iron(IV)-oxo model complexes have also been synthesized by using dioxygen[60] or hydrogen peroxide[61,62] as oxidants via mechanisms reminiscent of the O_2 and H_2O_2 activation process proposed in biology. Activation of O_2 at non-heme iron(II) model complexes has been achieved generally in the presence of additional electron and proton donors. Very recently, the role of sulphur donors in initiating a novel bimolecular activation of dioxygen at a model iron(II) center to generate an oxoiron(IV) species, reminiscent of the proposed O_2 activation mechanism in methane monooxygenase has also been demonstrated.[63] All the synthetic iron(IV)-oxo complexes show characteristic near-IR feature (λ_{max} = 600 – 1100 nm with ε = 100 – 450 M^{-1} cm^{-1}) in the absorption spectrum, which, on the basis of magnetic circular dichroism (MCD) studies,[64,65] have been assigned to ligand field-excited states originating from the d^4 Fe^{IV} center in both *S* = 1 and *S* = 2 states (Table 1 and SI, Table S1). In the *S* = 1 state the λ_{max} of this near-IR spectral Fe^{IV}=O signature is in general more blue-shifted than the *S* = 2 state, because of the higher destabilization of the d_{x2-y2} orbital relative to d_{xy}.

Detailed investigations on the reactivities of the reported iron(IV)-oxo complexes in HAT, OAT, and arene hydroxylation reactions have been carried out with both experimental and theoretical methods. In all of these studies, the spin states of the iron(IV)-oxo cores are shown to play a vital role in controlling the reactivity of the complexes. So far, all theoretical studies[66–71] have predicted that the Fe^{IV}=O species in the quintet state are better oxidants for HAT and aromatic hydroxylation reactions than those in the triplet state. The higher reactivity of the quintet state Fe^{IV}=O species is attributed to the limited steric interactions between the substrate and the Fe=O cores, because of the presence of a linear transition state involving a σ-attack of the substrate on the low-lying d_{z2} σ*-orbital. In contrast, in the triplet state, the d_{z2} σ*-orbital lies too high in energy, and hence is not available for interaction with the substrate. Accordingly, the reactivity of the iron(IV)-oxo in the *S* = 1 state is predicted to be quite low, as the steric interaction between the incoming substrate and the equatorial ligands of the iron(IV)-oxo core blocks access to the key $\pi^*(d_{xz/yz})$ frontier orbitals that are available for interaction with the substrate (Figure 3a). Nevertheless, the experimentally observed HAT reactivity of the *S* = 1 iron(IV)-oxo model complexes is much higher than that predicted from the theoretically-calculated activation barriers. Accordingly, a two-state-reactivity (TSR) model[68,70] was put forward, which postulates that the net activation barrier for the cleavage of a C−H bond by *S* = 1 iron(IV)-oxo complexes represents a weighted blend of the barrier on the ground triplet state and the excited quintet state surfaces. Thus, ligand-field effects that would decrease the energy gap between the ground triplet state and the excited quintet state are predicted to increase the rate of C−H bond cleavage by *S* = 1 iron(IV)-oxo complexes. Indeed, the three most reactive iron(IV)-oxo complexes in HAT reactions known to date possess either an *S* = 2 ground state (e.g., $[(TQA)Fe^{IV}(O)(CH_3CN)]^{2+}$ (TQA = tris(2-quinolylmethyl)amine))[57] or a highly reactive *S* = 2 excited state that lies in close proximity to the *S* = 1 ground state, such as in

$[(Me_3NTB)Fe^{IV}(O)]^{2+}$ (Me_3NTB = tris((*N*-methylbenzimidazol-2-yl)methyl)amine)[72] and $[(TMCO)Fe^{IV}(O)(CH_3CN)]^{2+}$ (TMCO = 4,8,12-trimethyl-1-oxa-4,8,12-triazacyclotetradecane)[73] (Figure 3a). Extremely weak equatorial donation from the co-ligand reduces the energy separation between the d_{x2-y2} and d_{xy} orbitals in these complexes, thereby stabilizing the S = 2 state. The nature of the axial donor groups can also control the reactivity of the iron(IV)-oxo cores. Increase in axial donation on one hand will increase the barrier for HAT at the S = 2 surface, owing to increasing energy of the acceptor d_{z2} orbital. At the same time, the d_{x2-y2} orbital will be stabilized with increasing axial donation,[74] thereby providing better access to the more reactive S = 2 state. These two contrasting effects lead to the increase of HAT reaction rates with increasing axial donation for the $[(TMC)Fe^{IV}(O)(X)]^{n+}$ (X = $NCCH_3$, CF_3COO^-, N_3^-, and RS^-) series[75] (Figure 3a), where the increase in the classical activation barrier is compensated by the effect of decreasing the triplet-quintet energy gap. In contrast, a different reactivity pattern is noted for the $[(TMC)Fe^{IV}(O)(CH_3CN)]^{2+}$, $[(TMC)Fe^{IV}(O)(CH_2CONMe_2)]^{2+}$, and $[(TMC)Fe^{IV}(O)(CH{=}C(O^-)NMe_2)]^+$ complexes[76] (Figure 3a), where the effect of destabilization of the d_{z2} orbital with increasing axial donation plays a dominant role in controlling the reactivity. In contrast to HAT where TSR predominates, OAT occurs via a single state and is controlled solely by the electrophilicity of the iron(IV)-oxo core.

In addition to TSR, the HAT ability of the iron–oxo cores can also be correlated with the strength of the O-H bond that forms after HAT.[77–79] In this regard, it has been shown that the rates of toluene oxidation by a series of oxygen-centered oxidants does not depend on the amount of radical character associated with the oxygen atom of the oxidant, but instead *correlates linearly* with the strength of the O−H bond formed upon reduction of the oxidant [D(O-H); Eq. 1, (where C is a constant)].[79]

$$D_{O\text{-}H} = 23.06\, E_{1/2} + 1.32\, pK_a + C \quad \ldots\ldots\ldots\ldots (1)$$

According to this equation the affinity (D(O-H) in kcal mol^{-1}) for HAT reaction of an iron(IV)-oxo complex is equivalent to its affinity for an electron (redox potential $E_{1/2}$ in V for the Fe^{IV}=O/Fe^{III}=O couple) and the affinity of the reduced iron(III)-oxo species for a proton (acid dissociation constant K_a of the conjugate base Fe^{III}−OH). Consistent with eq 1 the reactivity of the non-heme iron(IV)-oxo complexes can also be controlled by adding redox-innocent Lewis acid metal ions or protons, which results in a large positive shift of the $Fe^{IV/III}$ reduction potentials (E_{red}), thereby contributing to the enhancement of both HAT and OAT reaction rates.[80–87] The binding of Lewis acid metal ions can also activate an iron(IV)-oxo core for a radical-coupling O-O bond formation reaction with a hydroxide radical.[88] For example, an Fe^{IV}–O–Ce^{IV} species (Figure 3b), which is the closest structural and functional model for the essential heterodimetallic Mn^V–O–Ca^{II} centre involved in the water oxidation event in PS II, has been identified as the last detectable intermediate in Fe-catalyzed water oxidation reactions. A novel hexanuclear non-heme ligand system supported on a stannoxane core[89] has also been used as a suitable scaffold to preorganize two or more iron(IV)-oxo centers in a cofacial arrangement, thereby enforcing a radical-coupling O-O bond formation reaction.

The synthesized iron(IV)-oxo cores mostly exhibit moderate and noncatalytic reactivities, and they are often not kinetically competent to perform the rapid C-H or C=C oxidations observed in various catalysis systems based on iron(II) complexes of tetradentate N4-donor ligands and H_2O_2. The only exception is the $[(cyclam)Fe^{IV}(O)(CH_3CN)]^{2+}$ complex, which has been recently demonstrated to be a catalytically competent intermediate in the stereo- and regioselective epoxidation of olefins.[62] This study suggests that non-heme iron(IV)-oxo species cannot generally be excluded as viable intermediates in catalytic oxidation reactions.

In previous studies, iron(IV)-oxo cores have been excluded as the actual oxidants in iron-catalyzed epoxidation and *cis*-dihydroxylation reactions. An Fe^V(O)(OH) or Fe^V(O)(COOR) intermediate generated by O-O bond heterolysis of H_2O_2 at Fe(III) centers in the presence of

H_2O or carboxylic acids (RCOOH) is instead implicated as the active oxidant in such cases.[90] Notably, an $Fe^{V}(O)(OH)$ species formed by the isomerization of the Fe(III)-OOH precursor is also proposed as the active oxidant responsible for the hydroxylation of aryl C–H bonds, epoxidation, and *cis*-dihydroxylation of arenes in Rieske oxygenases.[91–94] However, direct evidence of such cores is lacking in biology. In contrast, in chemical oxidation reactions, few Fe(V)-oxo species have now been detected[36,95–97] under catalytic turnover conditions and characterized by a variety of low-temperature mass spectrometry (MS), electron paramagnetic resonance (EPR), Mössbauer, and isotopic labeling studies (Figure 3a and Table 1 and SI, Table S1). Fe(V)-oxo mediated O-O bond formation reactions have also been proposed during iron-catalyzed water oxidation reactions;[98] however, direct experimental evidence is lacking, thereby making the mechanism ambiguous.

In contrast to the wealth of synthetic iron(IV)-oxo (>80) and few iron(V)-oxo complexes[99–102] reported to date, stabilization of iron-oxo cores in other Fe oxidation states is extremely rare (Figure 3a). The only known example of an iron(VI) species is the tetrahedral $[Fe^{VI}O_4]^{2-}$ anion derived from mineral salts.[103] Two iron(III)-oxo species with a $(d_{x2-y2},d_{xy})^2(d_{xz})^1(d_{yz})^1(d_{z2})^1$ (S = 5/2) electronic configuration[104,105] have been crystallographically characterized by employing second-sphere hydrogen-bond donors to stabilize the terminal oxo unit within the trigonal ligand framework (Figure 3a). The effect of secondary H-bonding interactions and the low Fe-O bond order of only 0.5 are reflected in the low energy of the Fe-O stretch of 670 cm^{-1} for $[(H_3buea)Fe^{III}(O)]^{2-}$ (H_3buea = tris[(*N′-tert*-butylureaylato)-*N*-ethylene]aminato). Notably, the much higher energies of the Fe-O stretch for tetragonal $[(N4Py)Fe^{III}(O)]^{+}$ at 851 cm^{-1} and for trigonal $[(TPA)Fe^{III}(O)]^{+}$ at 856 cm^{-1} in the gas phase have been attributed to proposed S = 3/2 ground-states with electron configurations of $(d_{xy})^2(d_{xz})^1(d_{yz})^1(d_{x2-y2})^1$ and $(d_{x2-y2},d_{xy})^3(d_{xz})^1(d_{yz})^1$, respectively[106] (Table 1 and SI, Table S1). It is important to note that in $[(N4Py)Fe^{III}(O)]^{+}$ (Figure 2a), a formal Fe-O bond order of 2 (and hence Fe-O π-bonding) is achieved at the expense of the weakening of the Fe-pyridine(N) bonds in the equatorial plane, which represents a way to stabilize terminal metal-oxo cores with a d-electron count of greater than 4. Theoretical studies have also been performed to understand the trends in the HAT abilities of iron-oxo complexes as a function of the iron oxidation state. Here, the calculated reaction barrier decreases in the order of $Fe^{IV} > Fe^{V} > Fe^{VI}$ in the HAT reactivities of a series of iron(IV)-, iron(V)-, and iron(VI)-oxo complexes with a nearly identical coordination geometry.[107] However, in contrast to this theoretically predicted trend, $[(H_3buea)Fe^{III}(O)]^{2-}$ performs HAT at a much faster rate, compared to the corresponding $[(H_3buea)Fe^{IV}(O)]^{2-}$ complex[108] (Figure 3a). This puzzling reactivity pattern has been attributed to the high basicity of the $[(H_3buea)Fe^{III}(O)]^{2-}$ complex, which initiates a proton transfer prior to the electron transfer for the abstraction of a H-atom from a substrate. This is in contrast to $[(H_3buea)Fe^{IV}(O)]^{-}$, which abstracts a H-atom by a more traditional mechanism of near-concerted proton and electron transfer.

b. Terminal Manganese-Oxo Complexes

A number of manganese-oxo complexes have been synthesized and investigated for their ability to initiate O-O bond formation, HAT, and OAT reactions (see Figure 3b).[109,110] Mn(V)-oxo mediated O-O bond formation reactions have been demonstrated in two cases. One study reported that the reaction of Mn(V)-oxo corroles (corrole = tolylcorrole or nitrophenylcorrole) and hydroxide affords O_2 evolution;[111] the O-O bond formation in the reaction was demonstrated to occur via nucleophilic attack of the hydroxide ion on a Mn(V)-oxo moiety. Another study demonstrated a reversible O-O bond cleavage and an interconversion between high-valent Mn(V)-oxo and Mn(IV)-peroxo units, supported by a tris(3,5-tri-fluoromethylphenyl) corrole ligand, upon addition of hydroxide to a low-spin S = 0 Mn(V)-oxo species.[112] Similar to the Fe(V)-oxo cores, non-heme Mn(V)-oxo complexes generated by carboxylic acid-assisted heterolytic cleavage of Mn(III)-OOH species with two available *cis*-binding sites, which are formed from the reactions of Mn(II) precursors and H_2O_2, also act as efficient catalysts for

asymmetric epoxidation reactions.[113–119] Manganese complexes based on pentadentate non-heme ligands can also act as efficient epoxidation catalysts in the presence of PhIO as an oxidant.[119] Second-sphere hydrogen-bonding interactions between the H-atoms of the carboxylic acid and the oxo-group of the Mn(V)-oxo species presumably explain the formation of a highly reactive Mn(V)=O---H intermediate responsible for the enantioselective epoxidation reaction. The reactivity of the one-electron reduced Mn(IV)-oxo core has also been investigated, albeit in mostly non-catalytic HAT and OAT reactions.[120–124] A TSR reactivity is also evident in few well-characterized Mn(IV)-oxo cores, which have all been stabilized in the S = 3/2 ground state with an electronic configuration of $(d_{xy})^1(d_{xz})^1(d_{yz})^1(d_{x2-y2})^0(d_{z2})^0$. Notably, the lower effective nuclear charge of Mn, compared to Fe, ensures that the Mn d_{z2} orbital is placed at high energy so that the sterically less hindered σ-pathway is not available for HAT reactions. This contributes to the predominance of the steric control of Mn(IV)-oxo reactivity, and in general the lower reactivity of the Mn(IV)-oxo cores relative to the Fe(IV)-oxo cores. Accordingly, an inverse reactivity pattern is observed in the HAT reactivity of the Mn(IV)-oxo complexes supported by the bispidine BP1 and BP2 ligands,[125] relative to the analogous Fe(IV)-oxo complexes. In contrast to the higher HAT and OAT reactivities of the $[(BP2)Fe^{IV}(O)]^{2+}$ complex relative to $[(BP1)Fe^{IV}(O)]^{2+}$, owing to the higher Fe^{IV}/Fe^{III} reduction potential of the former, the corresponding $[(BP2)Mn^{IV}(O)]^{2+}$ complex was found to be less reactive than $[(BP1)Mn^{IV}(O)]^{2+}$ because of the higher steric demand of BP2 relative to BP1. Furthermore, a transition to the excited S = 1/2 state has been discussed as a prerequisite before any HAT reactions can occur. Thus, one way to increase the reactivity of the Mn(IV)=O core would be to stabilize the more reactive S = 1/2 state by tuning the ligand field at the Mn(IV) center.

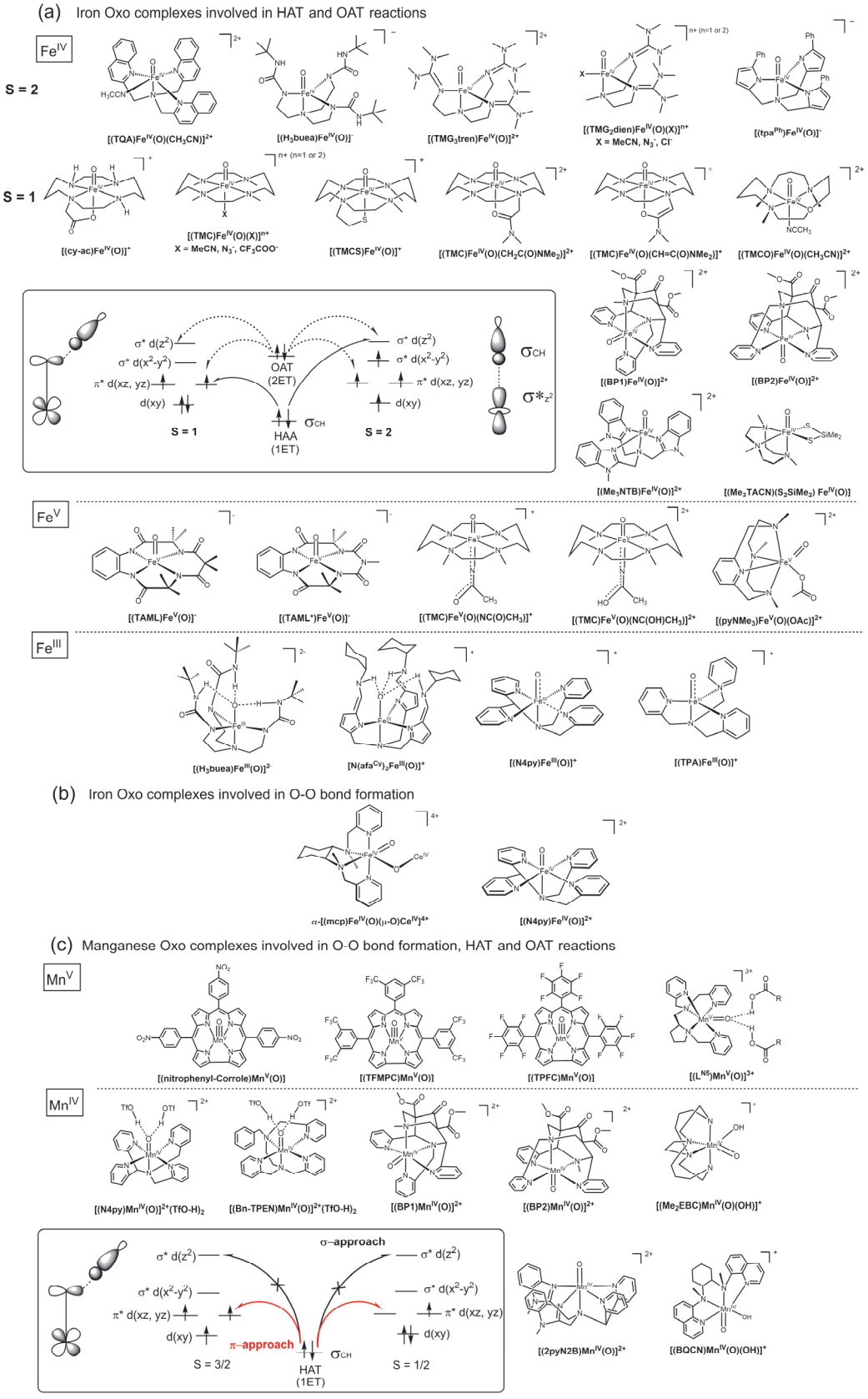
(a) Iron Oxo complexes involved in HAT and OAT reactions
Fe^IV
S = 2
S = 1
[(TQA)Fe^IV(O)(CH3CN)]2+
[(H3buea)Fe^IV(O)]-
[(TMG3tren)Fe^IV(O)]2+
[(TMG2dien)Fe^IV(O)(X)]n+
X = MeCN, N3-, Cl-
[(tpaPh)Fe^IV(O)]-
[(cy-ac)Fe^IV(O)]+
[(TMC)Fe^IV(O)(X)]n+
X = MeCN, N3-, CF3COO-
[(TMCS)Fe^IV(O)]+
[(TMC)Fe^IV(O)(CH2C(O)NMe2)]2+
[(TMC)Fe^IV(O)(CH=C(O)NMe2)]+
[(TMCO)Fe^IV(O)(CH3CN)]2+
σ* d(z2)
σ* d(x2-y2)
π* d(xz, yz)
d(xy)
OAT
(2ET)
σCH
S = 1
HAA
(1ET)
S = 2
σ*z2
[(BP1)Fe^IV(O)]2+
[(BP2)Fe^IV(O)]2+
[(Me3NTB)Fe^IV(O)]2+
[(Me3TACN)(S2SiMe2) Fe^IV(O)]
Fe^V
[(TAML)Fe^V(O)]-
[(TAML*)Fe^V(O)]-
[(TMC)Fe^V(O)(NC(O)CH3)]+
[(TMC)Fe^V(O)(NC(OH)CH3)]2+
[(pyNMe3)Fe^V(O)(OAc)]2+
Fe^III
[(H3buea)Fe^III(O)]2-
[N(afaCy)3Fe^III(O)]+
[(N4py)Fe^III(O)]+
[(TPA)Fe^III(O)]+
(b) Iron Oxo complexes involved in O-O bond formation
α-[(mcp)Fe^IV(O)(μ-O)Ce^IV]4+
[(N4py)Fe^IV(O)]2+
(c) Manganese Oxo complexes involved in O-O bond formation, HAT and OAT reactions
Mn^V
Mn^IV
[(nitrophenyl-Corrole)Mn^V(O)]
[(TFMPC)Mn^V(O)]
[(TPFC)Mn^V(O)]
[(L^N5)Mn^V(O)]3+
[(N4py)Mn^IV(O)]2+(TfO-H)2
[(Bn-TPEN)Mn^IV(O)]2+(TfO-H)2
[(BP1)Mn^IV(O)]2+
[(BP2)Mn^IV(O)]2+
[(Me2EBC)Mn^IV(O)(OH)]+
σ–approach
σ* d(z2)
σ* d(x2-y2)
π* d(xz, yz)
d(xy)
π–approach
σCH
S = 3/2
HAT
(1ET)
S = 1/2
[(2pyN2B)Mn^IV(O)]2+
[(BQCN)Mn^IV(O)(OH)]+

Figure 3. Structures of *S* = 2 and *S* = 1 Fe(IV)-oxo complexes discussed in this section and comparison of FMOs involved in the HAT and OAT reactions; selected structures of Fe(V)- and Fe(III)-oxo complexes (a); iron-oxo moieties involved in O-O bond formation (b); structures of selected Mn(V)- and Mn(IV)-oxo species involved in O-O bond formation, HAT, and OAT reactions and comparison between *S* = 1/2 and *S* = 3/2 Mn(IV)-oxo FMOs involved in HAT reactivity (c).

V. Mononuclear Late Transition Metal-Oxos

This section discusses the state-of-the-art in cobalt-, nickel-, and copper-oxo complexes. These complexes are unstable, as is predicted (section III), but have long been claimed as intermediates in reactions and catalytic cycles. Recently, researchers have stabilized and characterized a few putative metal-oxo complexes past the oxo wall.

a. Terminal Cobalt-Oxo Complexes

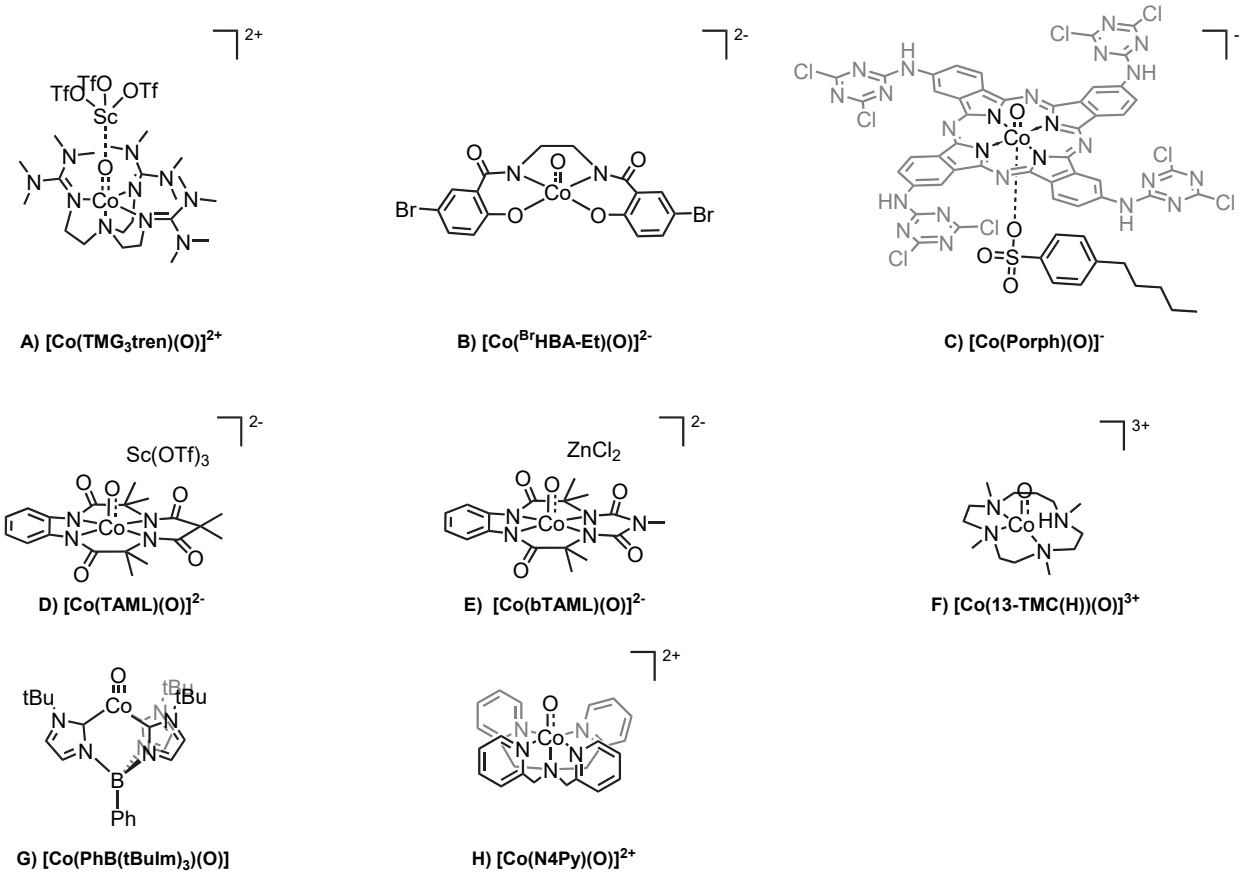

Figure 4. Structures of Co-oxo complexes discussed in this section.

High-valent Co-oxo complexes have been proposed as intermediates in several catalytic cycles (see Introduction). However, due to their high reactivity and instability, it has been challenging to isolate or observe them spectroscopically. Here we discuss Co-oxo complexes with some spectroscopic characterization, giving particular attention to how they inform our understanding of the Co-oxo bond. In 2013, a previous review on the subject described four complexes that are likely to be Co-oxo intermediates.[50] In particular, in 2011 $[Co(TMG_3tren)(O)]^{2+}$ (TMG_3tren = tris[2-(*N*-tetramethylguanidyl)ethyl]amine), with a cobalt-oxo bond that is stabilized by scandium(III) triflate, was reported.[46] This complex, shown in Figure 4A, has a TBP structure

and was characterized by X-ray absorption spectroscopy (XAS), extended X-ray absorption fine structure (EXAFS), EPR, and DFT calculations. Specifically, the EPR derived spin of S = 3/2 was proposed to support a hs complex with an electron configuration of $(d_{x2-y2},d_{xy})^3(d_{xz})^1(d_{yz})^1$. This supports a Co(IV)-O and not Co(III)-OH bond, as a Co(III)-OH species would have an electron configuration of $(d_{x2-y2},d_{xy})^4(d_{xz})^1(d_{yz})^1$, therefore having a spin of S = 2 and being EPR silent. In 2012, others proposed that this spin of S = 3/2 EPR signal was likely derived from remaining Co(II) in the sample, and that the species created was more likely Co(III) with a bridging hydroxide to the scandium ion.[126] It is also possible that a Co(III)-oxyl complex forms, but the crystal structure and IR spectra of the corresponding Co(III) complex with a bridging hydroxide to Ca^{2+} from the 2012 study suggest otherwise. Reactivity studies in both papers show hydrogen abstraction to aromatize organic molecules. In addition, the $[Co(TMG_3tren)(O)]^{2+}$ complex reported in 2011 shows an OAT reactivity.[46]

Since 2013, additional Co-oxo complexes have been claimed in further work. A new Co-oxo intermediate, $[Co(^{Br}HBA\text{-}Et)(O)]^{2-}$ ($H_4[^{Br}HBA\text{-}Et]$ = *N,N'*-(ethane-1,2-diyl)bis(5-bromo-2-hydroxybenzamide); see Figure 4B), was generated via peroxide cleavage or by oxo transfer, which then quickly reacts with C-H bonds of acetonitrile.[127] This is another example of C-H activation by a Co-oxo complex. A cobalt porphyrin covalently bound in a cellulose matrix was reported, as shown in Figure 4C.[128] In this study, the linear dodecylbenzenesulfonate as a proximal ligand was found to stabilize the proposed Co-oxo complex, by donating electron density to the cobalt center. Isolating the complex in the matrix further prevents self-degradation. In this way, the authors claimed to have stabilized a Co(IV)-oxo species, enough to briefly observe it in situ at room temperature. They observed an S = 1/2 EPR signal at g = 2.1 for the intermediate, which could correspond to a distorted octahedral ls Co(IV)-oxo complex. In terms of reactivity, this intermediate degrades dye effluents through oxo transfer reactions.

In 2014, a Co-oxo species with TAML (TAML = tetraamidomacrocyclic ligand) as a supporting ligand was reported.[129] In this study, a transient blue species was formed in solution, which they believed to be $[Co^{III}(TAML)(O\bullet)]^{2-}$ and which valence tautomerizes to the $[Co^{IV}(TAML)(O)]^{2-}$ complex when stabilized by a Lewis acid (LA; e.g., Sc^{3+} ion).[129] The latter is shown in Figure 4D. EPR confirmed that the complex in Figure 4D has an S = 1/2 ground state, as expected for a square-pyramidal ls complex with an electron configuration of $(d_{xy})^2(d_{xz},d_{yz})^3$. This would give a Co-O bond order of 1.5, and a very reactive Co-oxo/oxyl species. The complex was further characterized by UV-vis, XAS, and EXAFS. The best EXAFS fit assigned a Co-O distance of 1.67 Å, which is significantly shorter than the Co-O distance of 1.85 Å in $[Co(TMG_3tren)(O)]^{2+}$. Since LAs are necessary to stabilize the Co^{IV}-O core in both $[Co(TMG_3tren)(O)]^{2+}$ and $[Co^{IV}(TAML)(O)]^{2-}$; the shorter Co-O distance in $[Co^{IV}(TAML)(O)]^{2-}$ may imply the binding of the LA to the TAML coligand in contrast to the bridging Co^{IV}-O-LA core in $[Co(TMG_3tren)(O)]^{2+}$. Note that binding of LAs to TAML is not unprecedented in the literature; for example $Mn^{V}(O)(TAML)$ is reported to be activated for various oxidation reactions by binding LAs to the TAML backbone.[130] Reactivity studies show that $[Co^{IV}(TAML)(O)]^{2-}$ abstracts a H-atom from weaker C-H bonds and oxidizes thioanisole to thioanisole oxide. In 2016, another group modified the TAML ligand to give bTAML (bTAML = biuret-modified tetraamidomacrocyclic ligand), which includes a nitrogen in the ring as shown in Figure 4E.[131] Electrochemical evidence suggested formation of a highly oxidized Co-oxo species, and the UV-vis spectrum of this species matches the previously proposed $[Co^{IV}(TAML)(O)]^{2-}$ intermediate. Similarly, they found that a Lewis acid, $ZnCl_2$, was able to stabilize this species. This modified TAML ligand complex was used in water oxidation, and a Co(IV)-O species was suggested as a key intermediate.

As a note of caution, many of the ligands used to support Co-oxo complexes, especially TAML and its derivatives, are non-innocent (redox-active) ligands (L) that are able to form oxidized ligand radicals. This leads to uncertainties about the cobalt oxidation state, not only with respect to the Co(III)(O•)/Co(IV)(O) valence tautomerism, but in addition, also the

Co(III)(L•)/Co(IV)(L) valence tautomerism. This requires particularly careful studies to determine the true nature of the ground state of a putative Co(IV)-oxo complex. This may be the case in the putative $[Co^{IV}(TAML)(O)]^{2-}$ complex, as indicated in previous studies.[132,133] The blue species investigated above may therefore also involve an oxidized $[TAML^{3-\bullet}]$ radical or a [Co(TAML)]-type species, as reported previously.

A second note of caution, when Lewis acids are used to stabilize terminal metal-oxo species there is concern whether the resulting adduct is best described as a bridging oxo. Several examples show that Lewis acids can impact the reactivity of the metal-oxo intermediates.[134] On one hand, the Lewis acid – oxygen interaction could be electrostatic, or the LAs can bind to the coligand instead of the oxo ligand, and the metal-oxo complex can then be best described as terminal. This would make sense in the $[Co^{IV}(TAML)(O)]^{2-}$ case, where it has been proposed that the Co(III) is oxidized to Co(IV) upon interaction with the Sc^{3+}. On the other hand, careful investigation found scandium triflate's interaction with an electrophilic Fe(IV)-oxo complex caused reduction to the more basic Fe(III)-oxo species, which binds preferentially to Sc^{3+} and leads to the formation of an Fe^{III}-O-Sc^{3+} core.[135,136] Either way, these species help describe the Lewis acid interactions in PS II and indicate the initial (transient) formation of a terminal metal-oxo intermediate.

In 2017, a metastable Co(IV)-oxo species was prepared with a cobalt complex bearing the 13-TMC co-ligand and stabilized in the presence of a proton donor. This is the best characterized Co(IV)-oxo complex reported so far, including in-depth spectroscopic and theoretical studies (Figure 4F).[45] This species is metastable at –40 °C for ~3 h, allowing for further characterization and reactivity studies. In particular, rRaman spectroscopy shows the Co-O stretch at 770 cm^{-1}, which proves the presence of an oxo/oxyl ligand, and this Co-O unit was confirmed by MS. The coordination environment of the Co center was further investigated by EXAFS, giving average Co-N distances of 2.02 Å and a Co-O distance of 1.72 Å. EPR results were interpreted with an S = 3/2 ground state for the complex, which was further supported by theoretical investigations. Based on the latter, the valence electron configuration of the complex was assigned as $(d_{xy})^2(d_{xz},d_{yz})^2(d_{x2-y2})^1$, giving a formal Co-O bond order of 2 as discussed above. Reactivity studies show C-H activation of relatively weak C-H bonds and OAT reactions for this complex.

In 2018, a Co(III)-oxo species with a PTD ligand structure was reported.[137] By oxidizing and then deprotonating a Co(II)-OH species, the authors were able to isolate a Co(III)-oxo complex supported by Li^+ coordination. Precipitating a lithium salt then generates the terminal Co(III)-oxo species, [Co(PhB(tBuIm)$_3$)(O)] (PhB(tBuIm)$_3$ = tris(imidazol-2-ylidene)borate), shown in Figure 4G. This complex was characterized by X-ray crystallography and IR spectroscopy. DFT calculations suggests a $(d_{x2-y2})^2(d_{xy})^2(d_{z2})^2$ electronic configuration. Initial reactivity studies showed OAT and HAT abilities, and a related compound was investigated for electrochemical water oxidation.[138] A following study explored the C-H bond activation mechanism of the complex, finding evidence for an asynchronous proton-coupled electron transfer (PCET), where proton transfer to the basic oxo group precedes electron transfer.[139]

Most recently, the gas phase synthesis of $[Co^{IV}(N4Py)(O)]^{2+}$ (N4Py = N,N-bis(2-pyridylmethyl)-N-bis(2-pyridyl)methylamine) was reported, as shown in Figure 4H.[140] Electrospray ionization of $[Co^{III}(N4Py)(ClO_3)]^2$ resulted in the loss of ClO_2• and gave the desired complex as evidenced by MS. Helium-tagging IR photodissociation spectroscopy and DFT supported a weak Co-oxo bond (≤ 659 cm^{-1} stretch) and an electron configuration of $(d_{xy})^2(d_{yz}d_{xz})^3$, meaning that this complex is best described as a Co(III)-oxyl species. They similarly made and characterized the one electron reduced Co(III)-oxo species, which had a stronger Co-oxo bond (752 cm^{-1} stretch). In both cases, the Co-O stretches were confirmed through ^{18}O labeling studies.

b. **Terminal Nickel-Oxo Complexes**

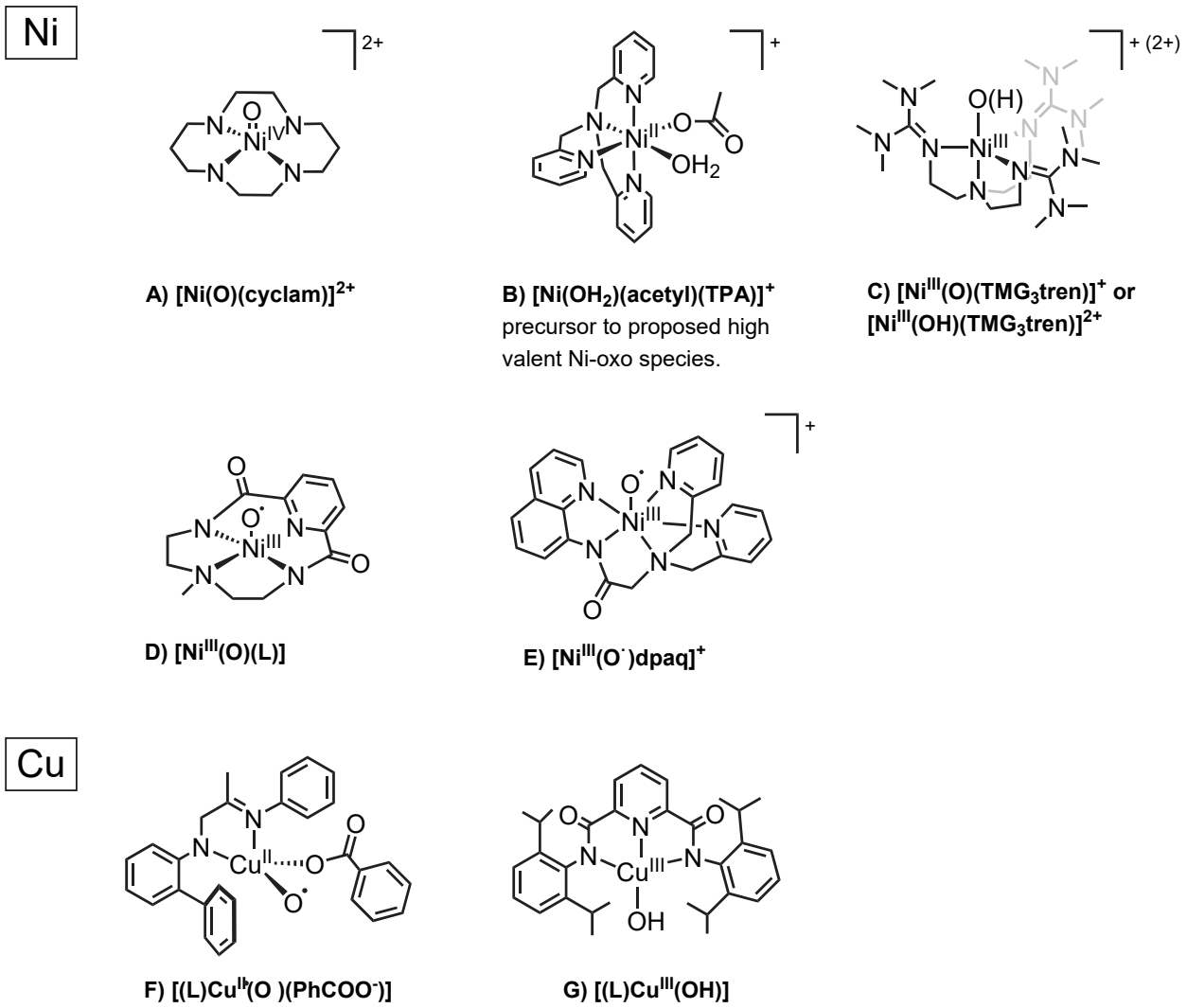

Figure 5. Structures of proposed nickel and copper complexes discussed in this section.

High-valent nickel–oxo complexes have also attracted much attention. Compared with analogous cobalt complexes, the extra electron further destabilizes the nickel-oxo bond making these unstable, highly reactive, and elusive complexes. Earlier reactivity studies have supported Ni(IV)-oxo species as plausible intermediates in a number of nickel catalyzed epoxidation and alkane hydroxylation reactions. In 1987, it was reported that nickel cyclam and similar complexes could perform olefin epoxidation when activated by PhIO, and a Ni(IV)-oxo intermediate was proposed (Figure 5A) as the active species.[141] A further exploration of this reaction showed that the intermediate had significant Ni(III)-oxyl character,[142] and in 2006 a nickel-oxo complex was suggested as the active species in alcohol formation when activated by *meta*-chloroperbenzoic acid (*m*CPBA) (the precursor $[Ni(OH_2)(acetyl)(TPA)]^+$ (TPA = tris(2-pyridylmethyl)amine) is shown in Figure 5B).[143,144] Additionally, the $[Ni^{III}–O]^+$ species is also suggested as a potent oxidant for the chemically challenging conversion of methane to methanol in the gas phase based on experimental[145–147] and theoretical studies.[146,148] However, no direct spectroscopic evidence for a high-valent nickel–oxo species has been reported until very recently, leaving the assignment ambiguous. The first stabilization of a Ni-oxo species was reported in 2012, as evidenced by EPR and UV-Vis spectroscopy.[149] The authors reported

formation of a $[Ni(III)(TMG_3tren)]^{3+}$ (TMG_3tren = tris[2-(N-tetramethylguanidyl)ethyl]amine) type species, which, based on its ability to perform oxo-transfer reaction and C–H activation with a rate-determining H-atom abstraction process, was assigned to a terminal Ni(III)–oxo/hydroxo complex in a TBP geometry, as shown in Figure 5C. This intermediate was formed by reacting the starting Ni(II) compound with *m*CPBA. EPR showed a total yield of 15% of Ni(III) species in solution, with 85% corresponding to one Ni(III) complex and 15% to a second species, each of which with a S = 1/2 ground state. These species are metastable with a half-life of 1 h at –30° C. The time course tracking of the EPR and UV-vis signals of these two intermediates matches, suggesting that they form and decay in similar ways or are somehow related. These intermediates are able to perform H-atom abstraction from 9,10-dihydroanthracene with a KIE value of 3.9, similar to that seen for the $[Ni(OH_2)(acetyl)(TPA)]^+$ catalyzed alkane hydroxylation reaction.[143] MS data did not show a Ni-oxo species but included reasonable degradation products.

Since 2012, research has continued toward isolating stable nickel-oxo species. In 2015, a Ni(III)-oxyl species, [Ni(III)(O)(L)] (L = bis(amidate) macrocycle, 6-methyl-3,6,9-triaza-1(2,6)-pyridinacyclodecaphane-2,10-dione), with a half-life of 4.5 h at –30° C was reported to be gererated by reacting the Ni(II) precursor with *m*CPBA (Figure 5D).[150] This intermediate exhibited UV-vis bands at 420 and 580 nm and two rhombic EPR signals with S = 1/2 for a total of 16% yield. However, formation rates for the Ni(III) species observed by EPR and the species observed by UV-vis are not the same. Instead, DFT studies suggest that the Ni(III)-oxyl species is EPR silent and that the species observed by EPR is a decay product. X-ray absorption near-edge structure (XANES) spectroscopy suggest Ni(III) as well. In addition, EXAFS shows two long N/O scatters at 2.12 Å and three short ones at 1.88 Å, which is evidence for an oxo or oxyl ligand weakly bound to the nickel center. rRaman shows bands at 450 and 477 cm^{-1} that they suggested originate from Ni-oxo species, but this was not confirmed with isotope labeling studies. This complex is able to react with thioanisole, activate weaker C-H bonds, and form epoxides from olefins. In 2016, $[Ni(O)(dpaq)]^+$ (dpaq = 2-(bis(pyridin-2-ylmethyl)amino)-N-(quinolin-8-yl)acetamide) was proposed to be formed by reacting the Ni(II) precursor with *m*CPBA in the catalytic epoxidation of olefins at room temperature (Figure 5E).[151] The authors proposed a mixture of Ni(III)- and Ni(IV)-oxo species based on reactivity studies with peroxyphenylacetic acid, where the decay products of the acid are characteristic for O-O bond breaking via homolysis or heterolysis, suggesting formation of a Ni(III)- or Ni(IV)-oxo species, respectively. This study proposed that Ni(IV)-oxo (74%) was formed along with Ni(III)-oxo (26%). EPR gave a Ni(III) species and MS is indicative of a Ni(IV)-oxo complex. However, it should be noted that no spectroscopic evidence for the proposed high-valent Ni intermediates was obtained in this study.

These examples show how Ni-oxo species have been suggested and supported by various groups in the literature, but solid evidence for these species is challenging to obtain, given their high reactivity and resistivity to being isolated. This makes it difficult for us to elucidate the exact geometric and electronic structures of these Ni species.

c. Terminal Copper-Oxo Complexes

The catalytic cycles of peptidylglycine α-hydroxylating monooxygenases (PHM) and dopamine β-monooxygenase (DβM) have attracted much attention in the communities of bioinorganic and biological chemistry but still remain controversial.[32,152,153] Different mechanisms have been proposed, but all of them incorporate the formation of mononuclear high-valent copper-oxo intermediates in the catalytic cycles. Nevertheless, a major subject of controversy is whether the generated copper-oxo units are reactive intermediates responsible for the hydroxylation of C-H bonds[154,155] or whether they are only formed after the HAT reactions mediated by Cu(II)-superoxo species and are then reduced via a PCET mechanism to regenerate the Cu(I) active state of the enzyme, which is responsible for O_2-activation.[156] Gas phase studies of $[CuO]^+$ have

shown its high reactivity for C-H activation,[157–162] but complexes stable enough for characterization in condensed phase are rare. An effort to investigate the potential of copper-oxo cores in initiating oxidative transformation reactions found that the oxidative decarboxylation pathway for substrate oxidations typically known for iron(II) α-ketocarboxylate active sites in enzymes can also be extended to the copper analogs.[163] Thus, a series of newly synthesized Cu(I) α-ketocarboxylate complexes performed arene hydroxylation reactions upon exposure to O_2; theoretical calculations implicated hydroxylation pathways that involve novel [Cu^{I}–OOC(O)R] and [Cu^{II}–O• ↔ Cu^{III}=O] species (Figure 5F). In particular, the ability of transient copper-oxo cores to induce the hydroxylation of arenes clearly establishes copper(III)-oxo/copper(II)-oxyl cores as viable intermediates during copper-mediated oxidation reactions. Copper-oxo mediated O-O bond formation reactions have also been suggested during copper-mediated O_2 generation.[19,164] The proposed copper-oxo intermediates in the above studies are, however, all too fleeting to be isolated. Very recently, the same group reported the isolation of LCuOH [L = *N*,*N*′-bis(2,6-diisopropylphenyl)-2,6-pyridinedicarboxamide] by one-electron oxidation of the tetragonal Cu^{II} complex [NBu_4][LCuOH] at –80 °C.[165] Subsequent XAS and DFT studies confirmed the presence of a Cu^{III}–OH moiety in [LCuOH] (Figure 5G). Notably, the stabilization of [LCuOH] further corroborates the applicability of the general strategy to stabilize late transition metal-oxo complexes via stabilizing interactions of nucleophilic oxo ligands with Lewis acidic redox-innocent metal ions or protons. [LCuOH], which can be considered as a tamed LCu-O species, was found to be a strong oxidant, and its HAT ability is significantly greater than that of most of the synthetic non-heme iron(IV)-oxo complexes. This is consistent with gas phase studies,[166] where $[CuO]^{+}$ ions were demonstrated to be better oxidants than the $[FeO]^{2+}$ analogs.

VI. Conclusions and Perspectives

In summary, the present review summarizes the versatile library of synthetic routes available to the synthetic chemist that has led to the isolation and in-depth characterization of a number of novel mononuclear terminal metal-oxo complexes and Lewis acid adducts of the oxo complexes of Mn, Fe, Co, Ni, and Cu. Successful synthetic strategies have mainly employed low-coordinate and non-tetragonal geometries and/or bulky ligands, which have helped to prevent the bimolecular decay pathways initiated by the highly basic oxo ligands of the metal-oxo cores. Further, equatorial donation of the ancillary ligands has been tuned to stabilize terminal metal-oxo cores beyond the so-called oxo-wall. In particular, the demonstrated stabilities and high OAT and HAA abilities of the tamed Lewis acid adducts of the otherwise transient Co^{IV}-O, Ni^{III}-O, and Cu^{III}-O cores corroborate their plausible involvement as reactive intermediates in Co, Ni and Cu catalyzed oxidation reactions. For the metals past the oxo wall, Co, Ni, and Cu, the initial analysis by Gray and co-workers in the 1960s predicted that the decrease in bond order makes the oxo ligand more reactive. The lack of stability of the Co- and Ni-oxo complexes described in this review suggests that this prediction holds and further indicates these complexes might be powerful oxidants with future applications in C-H activation and other useful reactions.

Convincing evidence is gathered based on reactivity studies of the synthesized metal-oxo cores that support the involvement of such intermediates in a number of metal-catalyzed HAT and OAT reactions that are well known in chemistry and biology. Secondary H-bonding interactions and spin states often play vital roles in improving the reaction rates and product yields and ensuring stereo-, regio-, and enantioselectivities. However, the reactions exhibited by the model metal-oxo complexes are mostly noncatalytic. One major problem is the non favorable oxygen rebound step and the preferable dissociation of the substrate radical (formed via the metal-oxo mediated HAT from hydrocarbons) to yield one electron reduced metal complex products, which cannot be further oxidized to regenerate the metal-oxo species. This

leads to a non-catalytic behavior, and an initiation of an autoxidation reaction by the substrate radical may occur. A fundamental understanding of the factors controlling the efficiency of the oxygen rebound step in nonheme metal-oxo systems is therefore warranted to achieve catalytic alkane hydroxylation reactions. Suitable ligand designs leading to the introduction of Lewis-acidic interaction in the secondary coordination sphere can not only result in enhanced metal-oxo mediated HAT rates but may also aid in the rebound step owing to the increasing electrophilicity of the Lewis-acid bound iron(III)-hydroxide species. For catalytic OAT reactions, on the other hand, the bimolecular decay pathway resulting from the reaction of the metal-oxo oxidant with the reduced metal complex formed after OAT to form the oxo-bridged dimetal thermodynamic sink should be avoided. Metal-oxo mediated O-O bond formation reactions have also been observed. Binding of metal-oxo cores to Lewis acidic centers or species possessing oxyl radical character has been discussed as the prerequisites necessary for the O-O bond formation step. However, the number of such examples is extremely rare and further studies are necessary before any definite reactivity trends for metal-oxo mediated O-O bond formation reactions can be established. Thus, new and innovative synthetic strategies and spectroscopic techniques are still needed to subdue thus far inaccessible oxo reactivities. Examples include the demonstration of the metal-oxo mediated methane oxidation reaction as well as trapping of metal-oxo cores under catalytic turnover conditions during the metal-mediated oxidation of water to dioxygen. The present review, in this context, provides a clear picture of the state-of-the-art as well as the insights into potential future synthetic endeavors; it may serve as a guide in making new types of synthetic metal-oxo cores and to the understanding of how they perform HAT, OAT, and O-O bond formation reactions.

Acknowledgements
The authors gratefully acknowledge the contributions of their collaborators and co-workers in the cited references. WN acknowledges the financial supports from the NRF of Korea through CRI (NRF-2012R1A3A2048842). NL acknowledges support for this work from the National Science Foundation (NSF, CHE-1900380). KR is funded by the Deutsche Forschungsgemeinschaft (DFG, German Research Foundation) under Germany's Excellence Strategy - EXC 2008 - 390540038 - UniSysCat and the Heisenberg-Professorship.

Author contributions
All authors contributed equally to the preparation of this manuscript.

Table 1: Summary of the selected spectroscopic properties of the early and late transition metal-oxos.[a]

Complex	M-O, Å EXAFS	ν(M=^{16}O) (^{18}O) cm^{-1}	Ref
Fe(IV) *S* = 2			
$[(TQA)Fe^{IV}(O)(CH_3CN)]^{2+}$	-	838 (803)	57
$[(H_3buea)Fe^{IV}(O)]^{-}$	1.680(1)	798 (765)	58
$[(TMG_3tren)Fe^{IV}(O)]^{2+}$	1.65	843 (810)	55
$[(TMG_2dien)Fe^{IV}(O)Cl]^{+}$	1.65	810 (775)	56
$[(TMG_2dien)Fe^{IV}(O)N_3]^{+}$	photodecom-position	833 (795)	56
$[(TMG_2dien)Fe^{IV}(O)CH_3CN]^{2+}$	1.65	807 (773)	56
$[(tpa^{Ph})Fe^{IV}(O)]^{-}$	1.65	FTIR 850 (814)	59
Fe(IV) *S* = 1 involved in O-O bond formation reaction			
$[(N_4py)Fe^{IV}(O)]^{2+}$	-	840 (806)	171
α-$[(mcp)Fe^{IV}(O)(\mu\text{-}O)Ce^{IV}]^{4+}$	-	822 (782) Fe=O, 677 (643) Fe-O-Ce	88
Fe(V) *S* = 1/2			
$[(TAML)Fe^{V}(O)]^{-}$	1.58	-	99
$[(TAML^{\bullet})Fe^{V}(O)]^{-}$	1.59	862 (824)	36, 100
$[(TMC)Fe^{V}(O)(CN(O)CH_3)]^{+}$	-	798 (763)	101
$[(TMC)Fe^{V}(O)(CN(OH)CH_3)]^{2+}$	-	811 (775)	101
$[(pyNMe_3)Fe^{V}(O)OAc]^{2+}$	1.63	-	102
Fe(III)			
$[(H_3buea)Fe^{III}(O)]^{2-}$, *S* = 5/2	1.81(3)	671 (645)	104
$[N(afa^{Cy})_3Fe^{III}(O)]^{+}$, *S* = 5/2	1.8079(9)	-	105
$[(N4py)Fe^{III}(O)]^{+}$, *S* = 3/2	-	851 (815)	106
$[(TPA)Fe^{III}(O)]^{+}$, *S* = 3/2	-	856 (820)	106
Mn(V) *S* = 0			
$[(TFMPC)Mn^{V}(O)]$	-	957 (920)	112
$[(TPFC)Mn^{V}(O)]$	-	958 (918)	109,172
Mn(IV) *S* = 3/2			
$[(N4py)Mn^{IV}(O)]^{2+}(TfOH)_2$	Mn-O-H 1.74 (Mn-O 1.673)	-	120
$[(Me_2EBC)Mn^{IV}(O)(OH)]^{+}$	1.7 (Mn=O), 1.84 (Mn-OH)	-	173
$[(2pyN2B)Mn^{IV}(O)]^{2+}$	1.671 (Mn=O) [b]	-	174
$[(BQCN)Mn^{IV}(O)(OH)]^{+}$	1.67/1.69 [b]	707 (676)	175
Co(IV)/Co(III)			
$[(TMG_3tren)Co^{IV}(O)]^{2+}$ *S* = 3/2	1.85	-	46
$[(TAML)Co^{IV}(O)]^{2-}$ *S* = 1/2	1.67	-	129
$[(13\text{-}TMC)Co^{IV}(O)]^{2+}$ *S* = 3/2	1.72	770 (736)	176
$[(PhB(tBuIm)_3)Co^{III}(O)]$ *S* = 0	XRD 1.682(6)	815 (782)	137
$[(N4Py)Co^{IV}(O)]^{2+}$ *S* = 1/2	-	≤659 (≤648)	140
Ni(III)			
$[(Lc^{b}Ni^{III}(O)]$, *S* = 1/2	2.12	450, 477	150
Cu(III)			
$[(L)^{d}Cu^{III}(OH)]$, *S* = 0	1.86	-	165

[a] See Supplementary Information for more spectroscopic information of metal-oxo complexes.

[b] DFT-computed distance.

[c] L = bis(amidate) macrocycle, 6-methyl-3,6,9-triaza-1(2,6)-pyridinacyclodecaphane-2,10-dione.

[d] L = *N*,*N*′-bis(2,6-diisopropylphenyl)-2,6-pyridinedicarboxamide.

References

1. Grätzel, M. Photoelectrochemical cells. *Nature* **414**, 338–344 (2001).
2. Lewis, N. S. & Nocera, D. G. Powering the planet: chemical challenges in solar energy utilization. *Proc. Natl. Acad. Sci. U. S. A.* **103**, 15729–35 (2006).
3. Gray, H. B. & Winkler, J. R. Living with Oxygen. *Acc. Chem. Res.* **51**, 1850–1857 (2018).
4. Borovik, A. S. Role of metal-oxo complexes in the cleavage of C-H bonds. *Chem. Soc. Rev*. **40**, 1870–1874 (2011).
5. Gunay, A. & Theopold, K. H. C-H Bond Activation by Metal-Oxo Compounds. *Chem. Rev.* **110**, 1060–1081 (2010).
6. Chen, Z. & Yin, G. The reactivity of the active metal oxo and hydroxo intermediates and their implications in oxidations. *Chem. Soc. Rev.* **44**, 1083–1100 (2015).
7. Betley, T. A., Wu, Q., Van Voorhis, T. & Nocera, D. G. Electronic Design Criteria for O−O Bond Formation via Metal−Oxo Complexes. *Inorg. Chem.* **47**, 1849–1861 (2008).
8. McEvoy, J. P. & Brudvig, G. W. Water-Splitting Chemistry of Photosystem II. *Chem. Rev,* **106**, 4455–4483 (2006).
9. Nam, W. Dioxygen Activation by Metalloenzymes and Models. *Acc. Chem. Res.* **40**, 465–465 (2007).
10. Bollinger, J. M. & Krebs, C. Enzymatic C–H activation by metal–superoxo intermediates. *Curr. Opin. Chem. Biol.* **11**, 151–158 (2007).
11. Hohenberger, J., Ray, K. & Meyer, K. The biology and chemistry of high-valent iron–oxo and iron–nitrido complexes. *Nat. Commun.* **3**, 720 (2012).
12. Engelmann, X., Monte-Pérez, I. & Ray, K. Oxidation Reactions with Bioinspired Mononuclear Non-Heme Metal-Oxo Complexes. *Angew. Chemie Int. Ed.* **55**, 7632–7649 (2016).
13. Ray, K., Pfaff, F. F., Wang, B. & Nam, W. Status of Reactive Non-Heme Metal-Oxygen Intermediates in Chemical and Enzymatic Reactions. *J. Am. Chem. Soc.* **136**, 13942–13958 (2014).
14. Guo, M., Corona, T., Ray, K. & Nam, W. Heme and Nonheme High-Valent Iron and Manganese Oxo Cores in Biological and Abiological Oxidation Reactions. *ACS Cent. Sci.* **5**, 13–28 (2019).
15. Armstrong, F. A. Why did Nature choose manganese to make oxygen? *Philos. Trans. R. Soc. B Biol. Sci.* **363**, 1263–1270 (2008).
16. Cox, N., Pantazis, D. A., Neese, F. & Lubitz, W. Biological Water Oxidation. *Acc. Chem. Res.* **46**, 1588–1596 (2013).
17. Pantazis, D. A. *et al.* Structure of the oxygen-evolving complex of photosystem II: information on the S_2 state through quantum chemical calculation of its magnetic properties. *Phys. Chem. Chem. Phys.* **11**, 6788–6798 (2009).
18. Cox, N. *et al.* Photosynthesis. Electronic structure of the oxygen-evolving complex in photosystem II prior to O-O bond formation. *Science* **345**, 804–808 (2014).
19. Kundu, S., Schwalbe, M. & Ray, K. Metal-oxo-mediated O-O bond formation reactions in chemistry and biology. *Bioinorg. React. Mech.* **8**, 41–57 (2012).
20. Yocum, C. F. The calcium and chloride requirements of the O_2 evolving complex. *Coord. Chem. Rev.* **252**, 296–305 (2008).
21. Siegbahn, P. E. M. Theoretical Studies of O−O Bond Formation in Photosystem II. *Inorg. Chem.* **47**, 1779–1786 (2008).
22. Siegbahn, P. E. . Mechanism and energy diagram for O–O bond formation in the oxygen-evolving complex in photosystem II. *Philos. Trans. R. Soc. B Biol. Sci.* **363**, 1221–1228 (2008).
23. Suga, M. *et al.* Light-induced structural changes and the site of O=O bond formation in PSII caught by XFEL. *Nature* **543**, 131–135 (2017).
24. Suga, M. *et al.* An oxyl/oxo mechanism for oxygen-oxygen coupling in PSII revealed by

an x-ray free-electron laser. *Science.* **366**, 334–338 (2019).
25. Nam, W., Lee, Y. M. & Fukuzumi, S. Tuning reactivity and mechanism in oxidation reactions by mononuclear nonheme iron(IV)-oxo complexes. *Acc. Chem. Res.* **47**, 1146–1154 (2014).
26. Poulos, T. L. Heme enzyme structure and function. *Chem. Rev*. **114,** 3919–3962 (2014).
27. Huang, X. & Groves, J. T. Oxygen Activation and Radical Transformations in Heme Proteins and Metalloporphyrins. *Chem. Rev.* **118**, 2491–2553 (2018).
28. Groves, J. T. & McClusky, G. A. Aliphatic hydroxylation via oxygen rebound. Oxygen transfer catalyzed by iron. *J. Am. Chem. Soc.* **98**, 859–861 (1976).
29. Riggs-Gelasco, P. J. *et al.* EXAFS Spectroscopic Evidence for an Fe=O Unit in the Fe(IV) Intermediate Observed during Oxygen Activation by Taurine:α-Ketoglutarate Dioxygenase. *J. Am. Chem. Soc.* **126**, 8108–8109 (2004).
30. Banerjee, R., Proshlyakov, Y., Lipscomb, J. D. & Proshlyakov, D. A. Structure of the key species in the enzymatic oxidation of methane to methanol. *Nature* **518**, 431–434 (2015).
31. Castillo, R. G. *et al.* High-Energy-Resolution Fluorescence-Detected X-ray Absorption of the Q Intermediate of Soluble Methane Monooxygenase. *J. Am. Chem. Soc.* **139**, 18024–18033 (2017).
32. Solomon, E. I. *et al.* Copper active sites in biology. *Chem. Rev*. **114**, 3659–3853 (2014).
33. Solomon, E. I. Dioxygen Binding, Activation, and Reduction to H_2O by Cu Enzymes. *Inorg. Chem.* **55**, 6364–6375 (2016).
34. Quist, D. A., Diaz, D. E., Liu, J. J. & Karlin, K. D. Activation of dioxygen by copper metalloproteins and insights from model complexes. *J. Biol. Inorg. Chem*. **22**, 253–288 (2017).
35. Keown, W., Gary, J. B. & Stack, T. D. P. High-valent copper in biomimetic and biological oxidations. *J. Biol. Inorg. Chem*. **22**, 289–305 (2017).
36. Kal, S., Xu, S. & Que, L. Bio-inspired Nonheme Iron Oxidation Catalysis: Involvement of Oxoiron(V) Oxidants in Cleaving Strong C−H Bonds. *Angew. Chemie Int. Ed.* (2019) doi:10.1002/anie.201906551.
37. Elwell, C. E. *et al.* Copper–Oxygen Complexes Revisited: Structures, Spectroscopy, and Reactivity. *Chem. Rev.* **117**, 2059–2107 (2017).
38. Nam, W., Lee, Y. M. & Fukuzumi, S. Hydrogen Atom Transfer Reactions of Mononuclear Nonheme Metal-Oxygen Intermediates. *Acc. Chem. Res.* **51**, 2014–2022 (2018).
39. Costas, M. Selective C-H oxidation catalyzed by metalloporphyrins. *Coordin. Chem. Rev*. **255**, 2912–2932 (2011).
40. Hay-Motherwell, R. S., Wilkinson, G., Hussain-Bates, B. & Hursthouse, M. B. Synthesis and X-ray crystal structure of oxotrimesityliridium(V). *Polyhedron* **12**, 2009–2012 (1993).
41. Poverenov, E. *et al.* Evidence for a terminal Pt(IV)-oxo complex exhibiting diverse reactivity. *Nature* **455**, 1093–1096 (2008).
42. Ballhausen, C. J. & Gray, H. B. The Electronic Structure of the Vanadyl Ion. *Inorg. Chem.* **1**, 111–122 (1962).
43. Winkler, J. R. & Gray, H. B. Electronic structures of oxo-metal ions. *Struct. Bond*. **142**, 17–28 (2012).
44. Gray, H. B. Elements of Life at the Oxo Wall. *Chem. Int.* **41**, 16–19 (2019).
45. Wang, B. *et al.* Synthesis and reactivity of a mononuclear non-haem cobalt(IV)-oxo complex. *Nat. Commun.* **8**, 14839 (2017).
46. Pfaff, F. F. *et al.* An Oxocobalt(IV) Complex Stabilized by Lewis Acid Interactions with Scandium(III) Ions. *Angew. Chem. Int. Ed.* **50**, 1711–1715 (2011).
47. Scepaniak, J. J. *et al.* Structural and Spectroscopic Characterization of an Electrophilic Iron Nitrido Complex. *J. Am. Chem. Soc.* **130**, 10515–10517 (2008).
48. Groysman, S., Villagran, D. & Nocera, D. G. Pseudotetrahedral d^0, d^1, and d^2 Metal-Oxo Cores within a Tris(alkoxide) Platform. *P. P. J. Organomet. Chem* **49**, 10759–10761

(2010).
49. Yamaguchi, K., Takahara, Y. & Fueno, T. Ab-Initio Molecular Orbital Studies of Structure and Reactivity of Transition Metal-OXO Compounds. *Applied Quantum Chemistry* 155–184 (Springer Netherlands, 1986).
50. Ray, K., Heims, F. & Pfaff, F. F. Terminal Oxo and Imido Transition-Metal Complexes of Groups 9-11. *Eur. J. Inorg. Chem.* **2013**, 3784–3807 (2013).
51. Decker, A. & Solomon, E. I. Dioxygen activation by copper, heme and non-heme iron enzymes: comparison of electronic structures and reactivities. *Curr. Opin. Chem. Biol.* **9**, 152–163 (2005).
52. Grapperhaus, C. A., Mienert, B., Eckhard, B., Weyhermüller, T. & Wieghardt, K. Mononuclear (Nitrido)iron(V) and (Oxo)iron(IV) Complexes via Photolysis of [(cyclam-acetato)$Fe^{III}(N_3)$]$^+$ and Ozonolysis of [(cyclam-acetato)$Fe^{III}(O_3SCF_3)$]$^+$ in Water/Acetone Mixtures. *Inorg. Chem* **39**, 5306–5317 (2000).
53. Rohde, J.-U. *et al.* Crystallographic and spectroscopic characterization of a nonheme Fe(IV)-O complex. *Science* **299**, 1037–1039 (2003).
54. Krebs, C., Fujimori, D. G., Walsh, C. T. & Bollinger, J. M. Non-heme Fe(IV)-oxo intermediates. *Acc. Chem. Res*. **40**, 484–492 (2007).
55. England, J. *et al.* A Synthetic High-Spin Oxoiron(IV) Complex: Generation, Spectroscopic Characterization, and Reactivity. *Angew. Chemie Int. Ed.* **48**, 3622–3626 (2009).
56. England, J. *et al.* A more reactive trigonal-bipyramidal high-spin oxoiron(IV) complex with a cis-labile site. *J. Am. Chem. Soc.* **133**, 11880–11883 (2011).
57. Biswas, A. N. *et al.* Modeling TauD-J : A High-Spin Nonheme Oxoiron(IV) Complex with High Reactivity toward C–H Bonds. *J. Am. Chem. Soc.* **137**, 2428–2431 (2015).
58. Lacy, D. C. *et al.* Formation, structure, and EPR detection of a high spin Fe^{IV}-Oxo Species Derived from Either an Fe^{III}-Oxo or Fe^{III}-OH Complex. *J. Am. Chem. Soc.* **132**, 12188–12190 (2010).
59. Bigi, J. P. *et al.* A high-spin iron(IV)-oxo complex supported by a trigonal nonheme pyrrolide platform. *J. Am. Chem. Soc.* **134**, 1536–1542 (2012).
60. Lee, Y.-M. *et al.* Dioxygen Activation by a Non-Heme Iron(II) Complex: Formation of an Iron(IV)−Oxo Complex via C−H Activation by a Putative Iron(III)−Superoxo Species. *J. Am. Chem. Soc.* **132**, 10668–10670 (2010).
61. Li, F., England, J. & Que, L. Near-Stoichiometric Conversion of H_2O_2 to Fe^{IV}=O at a Nonheme Iron(II) Center. Insights into the O−O Bond Cleavage Step. *J. Am. Chem. Soc.* **132**, 2134–2135 (2010).
62. Engelmann, X. *et al.* Trapping of a Highly Reactive Oxoiron(IV) Complex in the Catalytic Epoxidation of Olefins by Hydrogen Peroxide. *Angew. Chemie Int. Ed.* **58**, 4012–4016 (2019).
63. Gordon, J. B. *et al.* Activation of Dioxygen by a Mononuclear Nonheme Iron Complex: Sequential Peroxo, Oxo, and Hydroxo Intermediates. *J. Am. Chem. Soc.* **141**, 17533–17547 (2019).
64. Decker, A., Rohde, J.-U., Que, L. & Solomon, E. I. Spectroscopic and Quantum Chemical Characterization of the Electronic Structure and Bonding in a Non-Heme Fe^{IV}=O Complex. *J. Am. Chem. Soc* **126**, 5378–5379 (2004).
65. Srnec, M., Wong, S. D., England, J., Que, L. & Solomon, E. I. *π*-Frontier molecular orbitals in *S* = 2 ferryl species and elucidation of their contributions to reactivity. *Proc. Natl. Acad. Sci. U. S. A.* **109**, 14326–14331 (2012).
66. Shaik, S., Chen, H. & Janardanan, D. Exchange-enhanced reactivity in bond activation by metal–oxo enzymes and synthetic reagents. *Nat. Chem.* **3**, 19–27 (2011).
67. Wong, S. D. *et al.* Nuclear Resonance Vibrational Spectroscopy on the Fe^{IV}=O S=2 Non-Heme Site in TMG_3tren: Experimentally Calibrated Insights into Reactivity. *Angew. Chemie Int. Ed.* **50**, 3215–3218 (2011).

68. Hirao, H., Kumar, D., Que, L. & Shaik, S. Two-State Reactivity in Alkane Hydroxylation by Non-Heme Iron−Oxo Complexes. *J. Am. Chem. Soc.* **128**, 8590–8606 (2006).
69. Louwerse, M. J. & Jan Baerends, E. Oxidative properties of FeO^{2+}: electronic structure and solvation effects. *Phys. Chem. Chem. Phys.* **9**, 156–166 (2007).
70. Hirao, H., Que, L., Nam, W. & Shaik, S. A Two-State Reactivity Rationale for Counterintuitive Axial Ligand Effects on the C-H Activation Reactivity of Nonheme Fe^{IV}=O Oxidants. *Chem. - A Eur. J.* **14**, 1740–1756 (2008).
71. Janardanan, D., Wang, Y., Schyman, P., Que, L. & Shaik, S. The Fundamental Role of Exchange-Enhanced Reactivity in C-H Activation by *S*=2 Oxo Iron(IV) Complexes. *Angew. Chemie Int. Ed.* **49**, 3342–3345 (2010).
72. Seo, M. S. *et al.* A mononuclear nonheme iron(IV)-oxo complex which is more reactive than cytochrome P450 model compound I. *Chem. Sci.* **2**, 1039–1045 (2011).
73. Monte Pérez, I. *et al.* A Highly Reactive Oxoiron(IV) Complex Supported by a Bioinspired N_3O Macrocyclic Ligand. *Angew. Chemie Int. Ed.* **56**, 14384–14388 (2017).
74. Jackson, T. A. *et al.* Axial ligand effects on the geometric and electronic structures of nonheme oxoiron(IV) complexes. *J. Am. Chem. Soc.* **130**, 12394–12407 (2008).
75. Sastri, C. V *et al.* Axial ligand tuning of a nonheme iron(IV)-oxo unit for hydrogen atom abstraction. *Proc. Natl. Acad. Sci. U. S. A.* **104**, 19181–19186 (2007).
76. England, J. *et al.* An ultra-stable oxoiron(IV) complex and its blue conjugate base. *Chem. Sci.* **5**, 1204–1215 (2014).
77. Mayer, J. M. Hydrogen Atom Abstraction by Metal-Oxo Complexes: Understanding the Analogy with Organic Radical Reactions. *Acc. Chem. Res.* **31**, 441–450 (1998).
78. Cook, G. K. & Mayer, J. M. C-H Bond Activation by Metal Oxo Species: Chromyl Chloride Oxidations of Cyclooctane, Isobutane, and Toluene. *J. Am. Chem. Soc* **117**, 7139–7156 (1995).
79. Gardner, K. A., Kuehnert, L. L. & Mayer, J. M. Hydrogen Atom Abstraction by Permanganate: Oxidations of Arylalkanes in Organic Solvents. *Inorg. Chem.* **36**, 2069–2078 (1997).
80. Park, J., Lee, Y.-M., Nam, W. & Fukuzumi, S. Brønsted Acid-Promoted C–H Bond Cleavage via Electron Transfer from Toluene Derivatives to a Protonated Nonheme Iron(IV)-Oxo Complex with No Kinetic Isotope Effect. *J. Am. Chem. Soc.* **135**, 5052–5061 (2013).
81. Nishida, Y., Morimoto, Y., Lee, Y.-M., Nam, W. & Fukuzumi, S. Effects of Proton Acceptors on Formation of a Non-Heme Iron(IV)–Oxo Complex via Proton-Coupled Electron Transfer. *Inorg. Chem.* **52**, 3094–3101 (2013).
82. Park, J., Morimoto, Y., Lee, Y.-M., Nam, W. & Fukuzumi, S. Proton-Promoted Oxygen Atom Transfer vs Proton-Coupled Electron Transfer of a Non-Heme Iron(IV)-Oxo Complex. *J. Am. Chem. Soc.* **134**, 3903–3911 (2012).
83. Morimoto, Y. *et al.* Mechanistic Borderline of One-Step Hydrogen Atom Transfer versus Stepwise Sc^{3+}-Coupled Electron Transfer from Benzyl Alcohol Derivatives to a Non-Heme Iron(IV)-Oxo Complex. *Inorg. Chem.* **51**, 10025–10036 (2012).
84. Park, J. *et al.* Scandium Ion-Enhanced Oxidative Dimerization and *N*-Demethylation of *N*,*N*-Dimethylanilines by a Non-Heme Iron(IV)-Oxo Complex. *Inorg. Chem.* **50**, 11612–11622 (2011).
85. Park, J., Morimoto, Y., Lee, Y.-M., Nam, W. & Fukuzumi, S. Metal Ion Effect on the Switch of Mechanism from Direct Oxygen Transfer to Metal Ion-Coupled Electron Transfer in the Sulfoxidation of Thioanisoles by a Non-Heme Iron(IV)−Oxo Complex. *J. Am. Chem. Soc.* **133**, 5236–5239 (2011).
86. Morimoto, Y. *et al.* Metal Ion-Coupled Electron Transfer of a Nonheme Oxoiron(IV) Complex: Remarkable Enhancement of Electron-Transfer Rates by Sc^{3+}. *J. Am. Chem. Soc.* **133**, 403–405 (2011).

87. Fukuzumi, S. *et al.* Crystal structure of a metal ion-bound oxoiron(IV) complex and implications for biological electron transfer. *Nat. Chem.* **2**, 756–759 (2010).
88. Codolà, Z. *et al.* Evidence for an oxygen evolving iron–oxo–cerium intermediate in iron-catalysed water oxidation. *Nat. Commun.* **6**, 5865 (2015).
89. Kundu, S. *et al.* O–O Bond Formation Mediated by a Hexanuclear Iron Complex Supported on a Stannoxane Core. *Chem. - A Eur. J.* **18**, 2787–2791 (2012).
90. Cussó, O., Ribas, X. & Costas, M. Biologically inspired non-heme iron-catalysts for asymmetric epoxidation; design principles and perspectives. *Chem. Commun.* **51**, 14285–14298 (2015).
91. Kovaleva, E. G. & Lipscomb, J. D. Versatility of biological non-heme Fe(II) centers in oxygen activation reactions. *Nat. Chem. Biol.* **4**, 186–193 (2008).
92. Solomon, E. I., Goudarzi, S. & Sutherlin, K. D. O_2 Activation by Non-Heme Iron Enzymes. *Biochemistry* **55**, 6363–6374 (2016).
93. Costas, M., Mehn, M. P., Jensen, M. P. & Que, L. J. Dioxygen Activation at Mononuclear Nonheme Iron Active Sites: Enzymes, Models, and Intermediates. *Chem. Rev.* **104**, 939–986 (2004).
94. Que, L. & Tolman, W. B. Biologically inspired oxidation catalysis. *Nature* **455**, 333–340 (2008).
95. Lyakin, O. Y., Zima, A. M., Samsonenko, D. G., Bryliakov, K. P. & Talsi, E. P. EPR Spectroscopic Detection of the Elusive Fe^{V}═O Intermediates in Selective Catalytic Oxofunctionalizations of Hydrocarbons Mediated by Biomimetic Ferric Complexes. *ACS Catal.* **5**, 2702–2707 (2015).
96. Makhlynets, O. V. *et al.* H_2O_2 activation with biomimetic non-haem iron complexes and AcOH: connecting the g = 2.7 EPR signal with a visible chromophore. *Chem. Commun.* **50**, 645–648 (2014).
97. Lyakin, O. Y., Bryliakov, K. P. & Talsi, E. P. EPR, ^{1}H and ^{2}H NMR, and Reactivity Studies of the Iron–Oxygen Intermediates in Bioinspired Catalyst Systems. *Inorg. Chem.* **50**, 5526–5538 (2011).
98. Hong, Y. H. *et al.* Photodriven Oxidation of Water by Plastoquinone Analogs with a Nonheme Iron Catalyst. *J. Am. Chem. Soc.* **141**, 6748–6754 (2019).
99. De Oliveira, F. T. *et al.* Chemical and spectroscopic evidence for an Fe^{V}-oxo complex. *Science.* **315**, 835–838 (2007).
100. Ghosh, M. *et al.* Formation of a room temperature stable $Fe^{V}(O)$ complex: Reactivity toward unactivated C-H bonds. *J. Am. Chem. Soc.* **136**, 9524–9527 (2014).
101. Van Heuvelen, K. M. *et al.* One-electron oxidation of an oxoiron(IV) complex to form an $[O=Fe^{V}=NR]^{+}$ center. *Proc. Natl. Acad. Sci. U. S. A.* **109**, 11933–11938 (2012).
102. Serrano-Plana, J. *et al.* Trapping a Highly Reactive Nonheme Iron Intermediate That Oxygenates Strong C-H Bonds with Stereoretention. *J. Am. Chem. Soc.* **137**, 15833–15842 (2015).
103. Herren, M. & Guedel, H. U. Ferrate(VI), a novel near-infrared luminophore. *Inorg. Chem.* **31**, 3683–3684 (1992).
104. MacBeth, C. E. *et al.* O_2 activation by nonheme iron complexes: A monomeric Fe(III)-Oxo complex derived from O_2. *Science* **289**, 938–941 (2000).
105. Matson, E. M., Park, Y. J. & Fout, A. R. Facile Nitrite Reduction in a Non-heme Iron System: Formation of an Iron(III)-Oxo. *J. Am. Chem. Soc.* **136**, 17398–17401 (2014).
106. Andris, E. *et al.* Trapping Iron(III)–Oxo Species at the Boundary of the “Oxo Wall”: Insights into the Nature of the Fe(III)–O Bond. *J. Am. Chem. Soc.* **140**, 14391–14400 (2018).
107. Geng, C., Ye, S. & Neese, F. Does a higher metal oxidation state necessarily imply higher reactivity toward H-atom transfer? A computational study of C–H bond oxidation by high-valent iron-oxo and -nitrido complexes. *Dalt. Trans.* **43**, 6079 (2014).

108. Usharani, D., Lacy, D. C., Borovik, A. S. & Shaik, S. Dichotomous Hydrogen Atom Transfer vs Proton-Coupled Electron Transfer During Activation of X–H Bonds (X = C, N, O) by Nonheme Iron–Oxo Complexes of Variable Basicity. *J. Am. Chem. Soc.* **135**, 17090–17104 (2013).
109. Guo, M. *et al.* Dioxygen Activation and O–O Bond Formation Reactions by Manganese Corroles. *J. Am. Chem. Soc.* **139**, 15858–15867 (2017).
110. Young, K. J., Brennan, B. J., Tagore, R. & Brudvig, G. W. Photosynthetic Water Oxidation: Insights from Manganese Model Chemistry. *Acc. Chem. Res.* **48**, 567–574 (2015).
111. Gao, Y., Åkermark, T., Liu, J., Sun, L. & Åkermark, B. Nucleophilic Attack of Hydroxide on a Mn^{V}Oxo Complex: A Model of the O−O Bond Formation in the Oxygen Evolving Complex of Photosystem II. *J. Am. Chem. Soc.* **131**, 8726–8727 (2009).
112. Kim, S. H. *et al.* Reversible O−O Bond Cleavage and Formation between Mn(IV)-Peroxo and Mn(V)-Oxo Corroles. *J. Am. Chem. Soc.* **132**, 14030–14032 (2010).
113. Bryliakov, K. P. Catalytic Asymmetric Oxygenations with the Environmentally Benign Oxidants H_2O_2 and O_2. *Chem. Rev.* **117**, 11406–11459 (2017).
114. Bryliakov, K. P. & Talsi, E. P. Active sites and mechanisms of bioinspired oxidation with H_2O_2, catalyzed by non-heme Fe and related Mn complexes. *Coord. Chem. Rev.* **276**, 73–96 (2014).
115. Saisaha, P., de Boer, J. W. & Browne, W. R. Mechanisms in manganese catalysed oxidation of alkenes with H_2O_2. *Chem. Soc. Rev.* **42**, 2059–2074 (2013).
116. Wang, B., Miao, C., Wang, S., Xia, C. & Sun, W. Manganese Catalysts with C_1-Symmetric N_4 Ligand for Enantioselective Epoxidation of Olefins. *Chem. - A Eur. J.* **18**, 6750–6753 (2012).
117. Talsi, E. P. & Bryliakov, K. P. Chemo- and stereoselective CH oxidations and epoxidations/cis-dihydroxylations with H_2O_2, catalyzed by non-heme iron and manganese complexes. *Coord. Chem. Rev.* **256**, 1418–1434 (2012).
118. Ottenbacher, R. V., Bryliakov, K. P. & Talsi, E. P. Non-Heme Manganese Complexes Catalyzed Asymmetric Epoxidation of Olefins by Peracetic Acid and Hydrogen Peroxide. *Adv. Synth. Catal.* **353**, 885–889 (2011).
119. Du, J. *et al.* Mechanistic Insights into the Enantioselective Epoxidation of Olefins by Bioinspired Manganese Complexes: Role of Carboxylic Acid and Nature of Active Oxidant. *ACS Catal.* **8**, 4528–4538 (2018).
120. Chen, J. *et al.* Tuning the reactivity of mononuclear nonheme manganese(IV)-oxo complexes by triflic acid. *Chem. Sci.* **6**, 3624–3632 (2015).
121. Leto, D. F., Ingram, R., Day, V. W. & Jackson, T. A. Spectroscopic properties and reactivity of a mononuclear oxomanganese(IV) complex. *Chem. Commun.* **49**, 5378 (2013).
122. Chen, J. *et al.* A Mononuclear Non-Heme Manganese(IV)–Oxo Complex Binding Redox-Inactive Metal Ions. *J. Am. Chem. Soc.* **135**, 6388–6391 (2013).
123. Yoon, H., Morimoto, Y., Lee, Y.-M., Nam, W. & Fukuzumi, S. Electron-transfer properties of a nonheme manganese(IV)–oxo complex acting as a stronger one-electron oxidant than the iron(IV)–oxo analogue. *Chem. Commun.* **48**, 11187–11189 (2012).
124. Wang, Y., Shi, S., Wang, H., Zhu, D. & Yin, G. Kinetics of hydrogen abstraction by active metal hydroxo and oxo intermediates: revealing their unexpected similarities in the transition state. *Chem. Commun.* **48**, 7832–7834 (2012).
125. Barman, P. *et al.* Influence of Ligand Architecture on Oxidation Reactions by High-Valent Nonheme Manganese Oxo Complexes Using Water as a Source of Oxygen. *Angew. Chemie Int. Ed.* **54**, 2095–2099 (2015).
126. Lacy, D. C., Park, Y. J., Ziller, J. W., Yano, J. & Borovik, A. S. Assembly and Properties of Heterobimetallic $Co^{II/III}$/Ca^{II} Complexes with Aquo and Hydroxo Ligands. *J. Am. Chem.*

Soc. **134**, 17526–17535 (2012).
127. Nguyen, A. I., Hadt, R. G., Solomon, E. I. & Tilley, T. D. Efficient C–H bond activations via O_2 cleavage by a dianionic cobalt(II) complex. *Chem. Sci.* **5**, 2874–2878 (2014).
128. Li, N., Lu, W., Pei, K., Yao, Y. & Chen, W. Formation of high-valent cobalt-oxo phthalocyanine species in a cellulose matrix for eliminating organic pollutants. *Appl. Catal. B Environ.* **163**, 105–112 (2015).
129. Hong, S. *et al.* Spectroscopic Capture and Reactivity of a Low-Spin Cobalt(IV)-Oxo Complex Stabilized by Binding Redox-Inactive Metal Ions. *Angew. Chemie Int. Ed.* **53**, 10403–10407 (2014).
130. Hong, S. *et al.* A Manganese(V)-Oxo Complex: Synthesis by Dioxygen Activation and Enhancement of Its Oxidizing Power by Binding Scandium Ion. *J. Am. Chem. Soc.* **138**, 8523–8532 (2016).
131. Das, D., Pattanayak, S., Singh, K. K., Garai, B. & Sen Gupta, S. Electrocatalytic water oxidation by a molecular cobalt complex through a high valent cobalt oxo intermediate. *Chem. Commun.* **52**, 11787–11790 (2016).
132. Collins, T. J., Powell, R. D., Slebodnick, C. & Uffelman, E. S. Stable highly oxidizing cobalt complexes of macrocyclic ligands. *J. Am. Chem. Soc.* **113**, 8419–8425 (1991).
133. Popescu, D.-L. *et al.* High-valent first-row transition-metal complexes of tetraamido (4*N*) and diamidodialkoxido or diamidophenolato (2*N*/2*O*) ligands: Synthesis, structure, and magnetochemistry. *Coord. Chem. Rev.* **252**, 2050–2071 (2008).
134. Liu, Y. & Lau, T. C. Activation of Metal Oxo and Nitrido Complexes by Lewis Acids. *J. Am. Chem. Soc.* **141**, 3755–3766 (2019).
135. Swart, M. A change in the oxidation state of iron: Scandium is not innocent. *Chem. Commun.* **49**, 6650–6652 (2013).
136. Prakash, J. *et al.* Spectroscopic Identification of an Fe^{III} Center, not Fe^{IV}, in the Crystalline Sc−O−Fe Adduct Derived from $[Fe^{IV}(O)(TMC)]^{2+}$. *J. Am. Chem. Soc.* **137**, 3478–3481 (2015).
137. Goetz, M. K., Hill, E. A., Filatov, A. S. & Anderson, J. S. Isolation of a Terminal Co(III)-Oxo Complex. *J. Am. Chem. Soc.* **140**, 13176–13180 (2018).
138. McMillion, N. D. *et al.* Imidazole for Pyridine Substitution Leads to Enhanced Activity Under Milder Conditions in Cobalt Water Oxidation Electrocatalysis. *Inorg. Chem.* **58**, 1391–1397 (2019).
139. Goetz, M. K. & Anderson, J. S. Experimental Evidence for pK_a-Driven Asynchronicity in C–H Activation by a Terminal Co(III)–Oxo Complex. *J. Am. Chem. Soc.* **141**, 4051–4062 (2019).
140. Andris, E. *et al.* M−O Bonding Beyond the Oxo Wall: Spectroscopy and Reactivity of Cobalt(III)-Oxyl and Cobalt(III)-Oxo Complexes. *Angew. Chemie Int. Ed.* **58**, 9619–9624 (2019).
141. Koola, J. D. & Kochi, J. K. Nickel catalysis of olefin epoxidation. *Inorg. Chem.* **26**, 908–916 (1987).
142. Kinneary, J. F., Albert, J. S. & Burrows, C. J. Mechanistic studies of alkene epoxidation catalyzed by nickel(II) cyclam complexes. Oxygen-18 labeling and substituent effects. *J. Am. Chem. Soc.* **110**, 6124–6129 (1988).
143. Nagataki, T., Tachi, Y. & Itoh, S. Ni^{II}(TPA) as an efficient catalyst for alkane hydroxylation with m-CPBA. *Chem. Commun.* **38**, 4016–4018 (2006).
144. Nagataki, T., Ishii, K., Tachi, Y. & Itoh, S. Ligand effects on Ni^{II}-catalysed alkane-hydroxylation with m-CPBA. *Dalt. Trans.* 1120–1128 (2007).
145. Schröder, D. & Schwarz, H. C–H and C–C Bond Activation by Bare Transition-Metal Oxide Cations in the Gas Phase. *Angew. Chemie Int. Ed. English* **34**, 1973–1995 (1995).
146. Roithova, J. & Schröder, D. Selective Activation of Alkanes by Gas-Phase Metal Ions. *Chem. Rev.* **110**, 1170–1211 (2010).

147. Božović, A. *et al.* Conversion of Methane to Methanol: Nickel, Palladium, and Platinum (d^9) Cations as Catalysts for the Oxidation of Methane by Ozone at Room Temperature. *Chem. - A Eur. J.* **16**, 11605–11610 (2010).
148. Shiota, Y. & Yoshizawa, K. Methane-to-methanol conversion by first-row transition-metal oxide ions: ScO^+, TiO^+, VO^+, CrO^+, MnO^+, FeO^+, CoO^+, NiO^+, and CuO^+. *J. Am. Chem. Soc.* **122**, 12317–12326 (2000).
149. Pfaff, F. F., Heims, F., Kundu, S., Mebs, S. & Ray, K. Spectroscopic capture and reactivity of S = 1/2 nickel(III)–oxygen intermediates in the reaction of a Ni^{II}-salt with *m*CPBA. *Chem. Commun.* **48**, 3730–3732 (2012).
150. Corona, T. *et al.* Reactivity of a Nickel(II) Bis(amidate) Complex with *meta*-Chloroperbenzoic Acid: Formation of a Potent Oxidizing Species. *Chem. - A Eur. J.* **21**, 15029–15038 (2015).
151. Bok, K. H. *et al.* Synthesis, Characterization, and Catalytic Activities of A Nickel(II) Monoamido-Tetradentate Complex: Evidence For Ni^{III}-Oxo and Ni^{IV}-Oxo Species. *Chem. - A Eur. J.* **23**, 3117–3125 (2017).
152. Cowley, R. E., Tian, L. & Solomon, E. I. Mechanism of O_2 activation and substrate hydroxylation in noncoupled binuclear copper monooxygenases. *Proc. Natl. Acad. Sci. U. S. A.* **113**, 12035–12040 (2016).
153. Gherman, B. F., Heppner, D. E., Tolman, W. B. & Cramer, C. J. Models for dioxygen activation by the CuB site of dopamine *β*-monooxygenase and peptidylglycine α-hydroxylating monooxygenase. *J. Biol. Inorg. Chem.* **11**, 197–205 (2006).
154. Klinman, J. P. The copper-enzyme family of dopamine beta-monooxygenase and peptidylglycine alpha-hydroxylating monooxygenase: resolving the chemical pathway for substrate hydroxylation. *J. Biol. Chem.* **281**, 3013–6 (2006).
155. Crespo, A., Martí, M. A., Roitberg, A. E., Amzel, L. M. & Estrin, D. A. The Catalytic Mechanism of Peptidylglycine *α*-Hydroxylating Monooxygenase Investigated by Computer Simulation. *J. Am. Chem. Soc* **128**, 12817–12828 (2006).
156. Chen, P. & Solomon, E. I. Oxygen Activation by the Noncoupled Binuclear Copper Site in Peptidylglycine *α*-Hydroxylating Monooxygenase. Reaction Mechanism and Role of the Noncoupled Nature of the Active Site. *J. Am. Chem. Soc.* **126**, 4991 –5000 (2004).
157. Tsybizova, A. & Roithová, J. Copper-catalyzed reactions: Research in the gas phase. *Mass Spectrom. Rev.* **35**, 85–110 (2016).
158. Schröder, D., Holthausen, M. C. & Schwarz, H. Radical-like activation of alkanes by the ligated copper oxide cation (phenanthroline)CuO+. *J. Phys. Chem. B* **108**, 14407–14416 (2004).
159. Dietl, N., van der Linde, C., Schlangen, M., Beyer, M. K. & Schwarz, H. Diatomic $[CuO]^+$ and Its Role in the Spin-Selective Hydrogen- and Oxygen-Atom Transfers in the Thermal Activation of Methane. *Angew. Chemie Int. Ed.* **50**, 4966–4969 (2011).
160. Shaffer, C. J., Schröder, D., Gütz, C. & Lützen, A. Intramolecular C–H Bond Activation through a Flexible Ester Linkage. *Angew. Chemie Int. Ed.* **51**, 8097–8100 (2012).
161. Yassaghi, G., Andris, E. & Roithová, J. Reactivity of Copper(III)-Oxo Complexes in the Gas Phase. *ChemPhysChem* **18**, 2217–2224 (2017).
162. Srnec, M., Navrátil, R., Andris, E., Jašík, J. & Roithová, J. Experimentally Calibrated Analysis of the Electronic Structure of CuO^+: Implications for Reactivity. *Angew. Chemie Int. Ed.* **57**, 17053–17057 (2018).
163. Hong, S., Huber, S. M., Gagliardi, L. & Cramer, Christopher C Tolman, W. B. Copper(I)−α-Ketocarboxylate Complexes: Characterization and O_2 Reactions That Yield Copper−Oxygen Intermediates Capable of Hydroxylating Arenes. *J. Am. Chem. Soc.* **129**, 14190 –14192 (2007).
164. Halfen, J. A. *et al.* Reversible cleavage and formation of the dioxygen O-O bond within a dicopper complex. *Science.* **271**, 1397–1400 (1996).

165. Donoghue, P. J. *et al.* Rapid C–H Bond Activation by a Monocopper(III)–Hydroxide Complex. *J. Am. Chem. Soc.* **133**, 17602–17605 (2011).
166. Rijs, N. J., Weiske, T., Schlangen, M. & Schwarz, H. On divorcing isomers, dissecting reactivity, and resolving mechanisms of propane CH and aryl CX (X = halogen) bond activations mediated by a ligated copper(III) oxo complex. *Chem. Phys. Lett.* **608**, 408–424 (2014).
167. Sastri, C. V. *et al.* Axial ligand substituted nonheme Fe^{IV}=O complexes: Observation of near-UV LMCT bands and Fe=O Raman vibrations. *J. Am. Chem. Soc.* **127**, 12494–12495 (2005).
168. Rohde, J.-U. & Que, L. Axial Coordination of Carboxylate Activates the Non-heme Fe^{IV}=O Unit. *Angew. Chemie Int. Ed.* **44**, 2255–2258 (2005).
169. Bukowski, M. R. *et al.* Biochemistry: A thiolate-ligated nonheme oxoiron(IV) complex relevant to cytochrome P450. *Science.* **310**, 1000–1002 (2005).
170. Wang, D. *et al.* Nonheme oxoiron(IV) complexes of pentadentate N5 ligands: Spectroscopy, electrochemistry, and oxidative reactivity. *Chem. Sci.* **4**, 282–291 (2013).
171. Lee, Y.-M. *et al.* Water as an Oxygen Source in the Generation of Mononuclear Nonheme Iron(IV) Oxo Complexes. *Angew. Chemie Int. Ed.* **48**, 1803–1806 (2009).
172. Bougher, C. J., Liu, S., Hicks, S. D. & Abu-Omar, M. M. Valence Tautomerization of High-Valent Manganese(V)-Oxo Corrole Induced by Protonation of the Oxo Ligand. *J. Am. Chem. Soc.* **137**, 14481–14487 (2015).
173. Leto, D. F. & Jackson, T. A. Mn K-edge X-ray absorption studies of oxo- and hydroxo-manganese(IV) complexes: Experimental and theoretical insights into pre-edge properties. *Inorg. Chem.* **53**, 6179–6194 (2014).
174. Denler, M. C. *et al.* Mn^{IV}-Oxo complex of a bis(benzimidazolyl)-containing N5 ligand reveals different reactivity trends for Mn^{IV}-oxo than Fe^{IV}-oxo species. *Dalt. Trans.* **48**, 5007–5021 (2019).
175. Sawant, S. C. *et al.* Water as an Oxygen Source: Synthesis, Characterization, and Reactivity Studies of a Mononuclear Nonheme Manganese(IV) Oxo Complex. *Angew. Chemie Int. Ed.* **49**, 8190–8194 (2010).
176. Wang, B. *et al.* Synthesis and reactivity of a mononuclear non-haem cobalt(IV)-oxo complex. *Nat. Commun.* **8**, 14839 (2017).

TOC

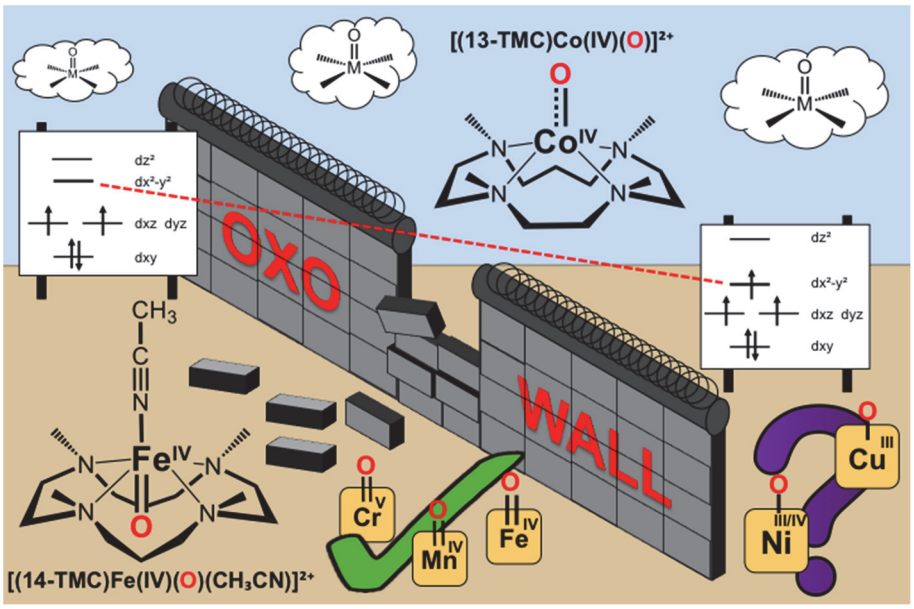

High-valent metal-oxo species are key intermediates in biological oxidation processes and implicated as active oxidants in industrially important reactions. This review highlights mononuclear iron- and manganese-oxo species, the nature of the “oxo wall”, and recent advances in late transition metal-oxo complexes.

ORCID
Kallol Ray: 0000-0003-2074-8844
Nicolai Lehnert: 0000-0002-5221-5498
Wonwoo Nam: 0000-0001-8592-4867